

SplineFlow: Flow Matching for Dynamical Systems with B-Spline Interpolants

Santanu Subhash Rathod¹ Pietro Liò² Xiao Zhang¹

Abstract

Flow matching is a scalable generative framework for characterizing continuous normalizing flows with wide-range applications. However, current state-of-the-art methods are not well-suited for modeling dynamical systems, as they construct conditional paths using linear interpolants that may not capture the underlying state evolution, especially when learning higher-order dynamics from irregular sampled observations. Constructing unified paths that satisfy multi-marginal constraints across observations is challenging, since naïve higher-order polynomials tend to be unstable and oscillatory. We introduce SplineFlow, a theoretically grounded flow matching algorithm that jointly models conditional paths across observations via B-spline interpolation. Specifically, SplineFlow exploits the smoothness and stability of B-spline bases to learn the complex underlying dynamics in a structured manner while ensuring the multi-marginal requirements are met. Comprehensive experiments across various deterministic and stochastic dynamical systems of varying complexity, as well as on cellular trajectory inference tasks, demonstrate the strong improvement of SplineFlow over existing baselines. Our code is available at: <https://github.com/santanurathod/SplineFlow>.

1. Introduction

Flow matching (Lipman et al., 2022) is a generative modeling technique with growing applications in a wide variety of domains, including biology (Li et al., 2025), spatial omics (Rathod et al., 2025), material sciences (Luo et al., 2025), and language modeling (Gat et al., 2024). This wide adoption results from the simplicity, scalability, and generality of its training process compared to existing generative tech-

niques, such as score-based diffusion (Song et al., 2020) and continuous normalizing flows (CNFs) (Chen et al., 2018b). Flow matching trains the velocity field of the underlying generative dynamics by *regressing* over a tractable conditional velocity field in a simulation-free manner, as opposed to several CNF-based techniques (Chen et al., 2018b; Rubanova et al., 2019) that require expensive simulations for training. At inference time, sampling in flow matching involves forward ODE integration steps, more efficient than the costly denoising steps of score-based diffusion (Song et al., 2020). Since accurately characterizing the velocity field lies at the heart of modeling dynamical systems, flow matching naturally provides a scalable probabilistic framework for learning the underlying continuous dynamics.

In the flow matching literature, conditional paths are typically constructed by *linearly interpolating* observed data points (Lipman et al., 2022; Zhang et al., 2024), which has been shown to generate high-fidelity samples with far fewer function evaluations (Pooladian et al., 2023). In these works, the primary emphasis is on the quality of generated samples, rather than on whether the learned dynamics meaningfully capture the true underlying dynamics. To faithfully model dynamical systems, the learned neural velocity field must closely match the underlying dynamics throughout the time horizon, rather than merely generating valid samples at observed time points. Since the neural velocity field is regressed on the conditional velocity field in flow matching, its faithfulness is limited by how closely the conditional paths approximate the underlying dynamics, making linear interpolants a restrictive design choice that is likely sub-optimal. This is especially true when data are irregularly sampled or when the underlying dynamics are nonlinear and contain exponential or sinusoidal terms, necessitating more flexible conditional paths to handle these cases. However, higher-degree polynomial paths satisfying all marginal observations tend to be oscillatory, a behavior known as Runge’s phenomenon (Epperson, 1987). Consequently, constructing higher-degree conditional paths that are stable, scalable, and easily integrated with existing frameworks remains challenging. While some prior work has focused on creating better conditional paths for modeling cellular dynamics using flow matching (Tong et al., 2024; Rathod et al., 2025), their emphasis has been on improving pairwise couplings while still relying on linear conditional paths.

¹CISPA Helmholtz Center for Information Security, Saarbrücken, Germany ²Department of Computer Science and Technology, University of Cambridge, Cambridge, UK. Correspondence to: Santanu Rathod <santanu.rathod@cispa.de>.

In this work, we present SplineFlow, a flow matching algorithm that constructs the conditional path using B-splines (Algorithm 1), a class of spline functions that are created using the Cox-de Boor recursion formula (De Boor & De Boor, 1978). Specifically, we elaborate on the limitations of using linear conditional paths for modeling complex dynamics and highlight the advantages of B-spline interpolants, including lower approximation errors, higher flexibility, and improved stability (Section 4.2). We illustrate how SplineFlow integrates B-spline conditional paths into the flow-matching framework, ensuring that the regressed velocity field satisfies the marginal distributions and enabling a more accurate characterization of the underlying dynamics (Section 4.3). Additionally, we extend our spline-based method to model stochastic dynamics with additive noise by regressing on both the drift and the score using simulation-free Schrödinger Bridges (Tong et al., 2023). Comprehensive experiments on simulations of both deterministic and stochastic dynamics with varying dimensionality, complexity, and sampling irregularity, as well as on real-world unpaired cellular trajectories, demonstrate that SplineFlow consistently outperforms existing flow matching baselines, especially when the observations are irregularly sampled (Section 5).

In summary, our contributions are as follows:

- Theoretically, we prove the function approximation error bounds of B-spline interpolants with comparisons to linear ones, showing that linear interpolants are a special case. We also demonstrate the validity of B-spline probability paths relative to existing flow matching frameworks, as well as the form of the associated conditional velocity field used during training.
- We introduce SplineFlow, a flow matching algorithm that uses B-splines to construct conditional probability paths for modeling deterministic dynamical systems, and a natural extension to the SF2M (score and flow matching) framework for stochastic systems.
- We provide extensive empirical evidence validating the advantages of SplineFlow across ODE dynamical systems and their stochastic counterparts of varying complexity, as well as cellular trajectory inference tasks under both interpolation and extrapolation settings.

2. Related Work

Flow Matching. Flow matching (Lipman et al., 2022; Albergo & Vandenberghe, 2022; Liu et al., 2022) is a probabilistic modeling framework for characterizing the generative dynamics by regressing a neural network on tractable conditional velocity fields, which bypasses expensive simulations as required in previous continuous normalizing flow techniques (Chen et al., 2018a; Papamakarios et al., 2021). Linear velocity fields are typically used in flow matching, as

they have been shown to achieve faster training convergence and greater efficiency in function evaluations than other choices, such as diffusion paths (Lipman et al., 2022; Liu et al., 2022). Notably, linear paths between noise and observations using optimal-transport couplings have resulted in even better performances (Pooladian et al., 2023). However, it's important to note that these techniques primarily optimize for endpoint generation fidelity and efficiency, and not for faithful characterization of intermediary dynamics.

Score Matching. In score-based diffusion models (Song et al., 2020; Nichol & Dhariwal, 2021), stochastic transformations are modeled by reversing a more tractable Gaussian-noising process, resulting in a score-dependent denoising velocity field. While capable of generating complex, high-dimensional data, its application to modeling stochastic dynamics is limited by its reliance on Gaussian-noise steps. Stochastically transforming two arbitrary distributions between each other is known as the Schrödinger Bridge problem (Léonard, 2013; Schrödinger, 1932) with several applications in generative modeling (De Bortoli et al., 2021; Vargas et al., 2021). However, the iterative methods for their approximate solutions (De Bortoli et al., 2021; Bunne et al., 2023) are known to suffer from stability and numerical issues limiting their applicability. To bridge these gaps, recent work (Tong et al., 2023) proposed modeling the stochastic dynamics by regressing probability flow velocity fields and probability scores over conditional probability paths modeled via Brownian bridges, again using linear interpolants.

Modeling System Dynamics. While the underlying state transformations of deterministic systems can be modeled by continuous normalizing flows (Chen et al., 2018a), these methods require computing an adjoint state via forward simulation at each iteration, which limits scalability. Similar requirements arise when modeling stochastic dynamics (Kidger et al., 2021) or dynamics from irregularly sampled observations (Rubanova et al., 2019). While flow matching has the potential to model dynamical systems in a scalable manner, thus far efforts to improve it on the dynamical front have been limited to solutions for modeling the processes underlying unpaired datasets, such as transcriptomic trajectories (Li et al., 2025). For instance, Tong et al. (2024) modeled the conditional paths between temporal transcriptomic samples by linearly interpolating between minibatch optimal transport (OT) couplings, while Rathod et al. (2025) achieved improvements by incorporating biological priors using spatial omics data. Zhang et al. (2024) employed flow matching for modeling dynamical systems, but they still rely on piecewise linear conditional paths, with no provision for faithfully characterizing the intermediary dynamics. While recent work (Rohbeck et al., 2025) proposed multi-marginal OT-couplings with cubic splines, it is primarily intended for deterministic modeling of unpaired transcriptomic datasets,

lacking rigorous guarantees regarding the choice and flexibility to convert to lower-order polynomials when needed. In contrast, SplineFlow is the first method to demonstrate the efficacy of modeling dynamics across degrees of complexity using well-motivated B-spline interpolants.

3. Preliminaries

Flow Matching (FM). Flow matching (Lipman et al., 2022) is a technique that characterizes continuous normalizing flows for a system of variables. Let $\psi : [0, 1] \times \mathbb{R}^d \rightarrow \mathbb{R}^d$ be the underlying continuous flow that acts on random variables at each time $t \in [0, 1]$. Specifically, it transforms samples x_0 from the source distribution $q_0 = q(x_0)$ into samples x_1 from the target distribution $q_1 = q(x_1)$, so that $\psi(1, x_0) = x_1$. In continuous normalizing flows, ψ can be defined by an ordinary differential equation (ODE):

$$\frac{d\psi(t, x_0)}{dt} = \frac{dx_t}{dt} = u_t(x_t), \quad (1)$$

where $u_t(x_t) : [0, 1] \times \mathbb{R}^d \rightarrow \mathbb{R}^d$ is the velocity field describing the rate of change of the random variables. Transforming the random variable x_t also transforms the associated probability distribution $p_t(x) : [0, 1] \times \mathbb{R}^d \rightarrow \mathbb{R}_+$, which satisfies the boundary conditions $p_{t=0} = q(x_0)$ and $p_{t=1} = q(x_1)$. The relationship between the velocity field and its induced probability distribution at time t is given by the well-known *continuity equation* (Villani et al., 2008):

$$\frac{\partial p_t(x)}{\partial t} = -\nabla_x \cdot (u_t(x)p_t(x)), \quad (2)$$

where ∇_x denotes the divergence operator. Flow matching approximates the velocity field by a neural network $u_\theta : [0, 1] \times \mathbb{R}^d \rightarrow \mathbb{R}^d$ by minimizing a regression loss \mathcal{L}_{FM} :

$$\min_{\theta} \mathbb{E}_{t \sim \mathcal{U}(0,1), x \sim p_t(x)} \|u_\theta(t, x) - u_t(x)\|^2, \quad (3)$$

where $\mathcal{U}(0, 1)$ denotes the uniform distribution over $[0, 1]$, and p_t is the time-varying probability distribution induced by the velocity field u_t . Once trained, the velocity field u_θ can be integrated from 0 to 1 to transform a source sample $x_0 \sim q_0$ into a target sample $x_1 \sim q_1$. In practice, however, the velocity field $u_t(x)$ is unknown, and several velocity fields can exist such that the boundary conditions for the induced probability paths are satisfied.

Conditional Flow Matching (CFM). To tackle the intractability of the flow matching objective \mathcal{L}_{FM} in Equation 3, conditional flow matching (Lipman et al., 2022) was introduced, where the velocity field $u_t(x)$ and the induced probability path $p_t(x)$ are defined as:

$$p_t(x) = \int p_t(x | z)q(z)dz, \quad (4)$$

$$u_t(x) = \int u_t(x | z) \frac{p_t(x | z)q(z)}{p_t(x)} dz. \quad (5)$$

Here, z is the conditional latent variable with probability distribution $q(z)$, with $u_t(x | z)$ being the conditional velocity fields defined such that the induced conditional probability paths $p_t(x | z)$ satisfy the distributions at boundaries, or $\int p_{t=0}(x | z)q(z)dz = q_0$ and $\int p_{t=1}(x | z)q(z)dz = q_1$. The CFM regression loss \mathcal{L}_{CFM} can then be written as:

$$\min_{\theta} \mathbb{E}_{t \sim \mathcal{U}(0,1), z \sim q(z), x \sim p_t(x | z)} \|u_\theta(t, x) - u_t(x | z)\|^2. \quad (6)$$

Lipman et al. (2022) proved that $\nabla_{\theta} \mathcal{L}_{\text{FM}} = \nabla_{\theta} \mathcal{L}_{\text{CFM}}$, suggesting that we can regress the velocity field using the more tractable conditional velocities but still recover the solution from Equation 3. Therefore, the remaining task is to define an appropriate conditional velocity field $u_t(x | z)$ and the associated probability path $p_t(x | z)$ to sample from.

In the prior flow matching literature, the conditional path $p_t(x | z)$ is often modeled using a Gaussian distribution with $\mu_t(z)$ and $\sigma_t(z)$ being the constructed, latent-dependent, time-varying mean and standard deviation, such that the distribution at a sampled time point matches the observations. For such a particular choice, the associated conditional velocity $u_t(x | z)$ can be expressed in an analytical form:

$$p_t(x | z) = \mathcal{N}(x | \mu_t(z), \sigma_t(z)^2), \quad (7)$$

$$u_t(x | z) = \frac{\sigma'_t(z)}{\sigma_t(z)}(x - \mu_t(z)) + \mu'_t(z). \quad (8)$$

Flow And Score Matching (SF2M). In certain scenarios, the underlying dynamics of the state random variables x_t can evolve stochastically, corresponding to a stochastic differential equation (SDE):

$$dx_t = u_t(x_t)dt + g(t)dw_t, \quad (9)$$

where $u_t(x) : [0, 1] \times \mathbb{R}^d \rightarrow \mathbb{R}^d$ is the velocity field, $g(t) : [0, 1] \rightarrow \mathbb{R}_{>0}$ is a positive diffusion function, and w_t stands for the standard Wiener process. The relationship between $u_t(x)$ and the SDE induced probability path $p_t(x) : [0, 1] \times \mathbb{R} \rightarrow \mathbb{R}_+$ is given by a *Fokker-Planck equation* (FPE):

$$\frac{\partial p_t(x)}{\partial t} = -\nabla_x \cdot (u_t(x)p_t(x)) + \frac{g^2(t)}{2} \nabla_x^2(p_t(x)). \quad (10)$$

Song et al. (2020) showed that starting from some initial distribution $p_0(x)$ and evolving the random variable according to the probability flow ODE with drift $u_t^o(x_t)$:

$$dx_t = \left[u_t(x_t) - \frac{g^2(t)}{2} \nabla_x \log(p_t(x_t)) \right] dt = u_t^o(x_t)dt, \quad (11)$$

induces the same time varying marginal distribution $p_t(x)$ as the SDE defined by Equation 9. Therefore, given a diffusion schedule $g(t)$, the score function $\nabla_x \log(p_t(x_t))$, and the

drift $u_t^o(x_t)$ defined by Equation 11, we can recover the drift for the original SDE in Equation 9 as:

$$u_t(x_t) = u_t^o(x_t) + \frac{g^2(t)}{2} \nabla_x \log(p_t(x_t)). \quad (12)$$

Analogous to conditional flow matching, the drift $u_t^o(x)$ and the score $\nabla_x \log(p_t(x))$ can be approximated by neural networks optimizing the following regression loss over their conditional equivalents (Theorem 3.2 in Tong et al. (2023)):

$$\begin{aligned} \mathcal{L}_{\text{SF2M}}(\theta, \phi) = & \mathbb{E}_{t, z, x} \left[\|u_\theta(t, x) - u_t^o(x | z)\|^2 \right. \\ & \left. + \lambda(t)^2 \|s_\phi(t, x) - \nabla \log p_t(x | z)\|^2 \right]. \end{aligned} \quad (13)$$

Here, $u_t^o(x | z)$ induces the conditional probability $p_t(x | z)$ and the expectation is taken over uniformly distributed time $t \sim \mathcal{U}(0, 1)$, the latent variables $z \sim q(z)$ and the conditional probability samples $x \sim p_t(x | z)$, and $\lambda(t)$ denotes the time conditional weights. When the conditional probability path is constructed as a linear Brownian bridge:

$$p_t(x | z) = \mathcal{N}(x; (1-t)x_0 + tx_1, \sigma^2 t(1-t)), \quad (14)$$

where $z = (x_0, x_1)$ is the conditional variable, then according to Equation 8, the drift and the score are given by:

$$\begin{aligned} u_t^o(x | z) &= \frac{1-2t}{t(1-t)} (x - tx_1 - (1-t)x_0) + x_1 - x_0, \\ \nabla_x \log p_t(x) &= \frac{tx_1 + (1-t)x_0 - x}{\sigma^2 t(1-t)}. \end{aligned} \quad (15)$$

4. Flow Matching for Dynamical Systems

4.1. Problem Setup

While flow matching algorithms are primarily designed to optimize endpoint data generation ($t = 1$), they have been extended to characterize the underlying dynamics of complex dynamical systems, where observations are made at multiple time points, potentially across different trajectories. More formally, let x_t denote the state variables of the underlying dynamics at time t governed either by an ODE $dx_t = u_t(x_t)dt$ if the dynamical system is deterministic, or by a SDE $dx_t = u_t(x_t)dt + g(t)dw_t$ if stochastic. Here, $u_t(\cdot)$ is the unknown velocity or drift, $g(t)$ stands for the diffusion schedule, and w_t is the standard Wiener process.

Let $\{X_i\}_{i=0}^{N-1}$ be a collection of N training trajectories that follow the state evolution dynamics defined by an ODE or SDE but with different initial values, where the i -th trajectory $X_i = [x_i(t_0^i), x_i(t_1^i), \dots, x_i(t_{n_i}^i)]$, $x_i(t_j^i) \in \mathbb{R}^d$ denotes the j -observation within the i -th trajectory, $x_i(t_0^i)$ stands for the initial value, and $t_0^i < t_1^i < \dots < t_{n_i}^i$ are the observed timestamps. Note that the observed timestamps $\{t_0^i, t_1^i, \dots, t_{n_i}^i\}$ can vary across different trajectories.

Additionally, we use $p \in [0, 1]$ to denote the degree of irregularity of the sampled timestamps. In our experiments, we randomly mask a fraction p of observations from each training trajectory. The objective is to learn a neural network v_θ to approximate the underlying system dynamics (also a score network s_ϕ for SDE). More precisely, for any unseen trajectory X_{te} that follows the same underlying state evolution dynamics x_t as the training ones, the goal is to minimize the mean square error (MSE) between the predicted and ground-truth observations across any set of timestamps.

4.2. Advantages of B-Spline Interpolants

In prior literature on flow matching (Zhang et al., 2024; Tong et al., 2024), the neural network is typically trained by regressing on conditional velocity fields that generate Gaussian conditional paths, using learning interpolants for each consecutive observation pair. To be more specific, for any training trajectory X_i , the conditional probability any time $t \in [t_j^i, t_{j+1}^i]$ are defined as:

$$\begin{aligned} p_t(x | z) &= \mathcal{N}(x; \mu_t(z), \sigma^2 I), \text{ where} \\ \mu_t(z) &= \frac{t_{j+1}^i - t}{t_{j+1}^i - t_j^i} x_i(t_j^i) + \frac{t - t_j^i}{t_{j+1}^i - t_j^i} x_i(t_{j+1}^i), \end{aligned} \quad (16)$$

where $z = (x_i(t_j^i), x_i(t_{j+1}^i))$ is the latent variable and $\sigma \ll 1$ is a small constant denoting the standard deviation. Similar to Equation 8, we can derive the corresponding conditional velocity field $u_t(x | z) = [x_i(t_{j+1}^i) - x_i(t_j^i)] / (t_{j+1}^i - t_j^i)$.

Since linear probability paths interpolate between observational points, the trained velocity field will induce a marginal distribution that is approximately similar to the observational distribution, thus modeling the underlying dynamics. However, while linear paths connect observations at endpoints they don't approximate the intermediary functional values well, and in particular, often miss out on curvature and induce significant bias, as illustrated in Figure 1.

B-Spline Interpolants. Witnessing the above limitations of linear interpolants, we propose constructing the conditional paths using B-spline interpolants to faithfully capture the complex underlying system dynamics. B-Splines are widely used to model complex shapes and functions across several domains (Hasan et al., 2024), including computer graphics and computer-aided design (CAD), among others (Biswas & Lovell, 2008; Li, 2020). Notably, B-splines are known to be stable, smooth, and flexible with respect to the choice of polynomial degree, whereas other alternative choices of higher-order interpolants are prone to oscillatory behavior such as Runge's phenomenon (Epperson, 1987) and to non-smoothness (see Appendix B for more detailed discussions).

Let $[x_{t_0}, x_{t_1}, \dots, x_{t_n}]$ be the $n + 1$ points we need to interpolate over, B-spline Interpolant function is built over by recursively combining basis splines using the Cox-De

Boor Recursion formula (De Boor & De Boor, 1978). More formally, the 0-th degree B-spline basis is defined as:

$$\mathcal{B}_{j,0} = \begin{cases} 1 & \text{if } t \in [t_j, t_{j+1}), \\ 0 & \text{otherwise.} \end{cases} \quad (17)$$

Higher-degree B-spline bases are defined recursively by:

$$\begin{aligned} \forall m \geq 1, \quad \mathcal{B}_{j,m}(t) &= \frac{t - t_j}{t_{j+m} - t_j} \mathcal{B}_{j,m-1}(t) \\ &+ \frac{t_{j+m+1} - t}{t_{j+m+1} - t_{j+1}} \mathcal{B}_{j+1,m-1}(t). \end{aligned} \quad (18)$$

The interpolant function $\mu(t)$ of degree m is then a linear combination of m -th degree B-splines, such that it recovers the $n + 1$ observation points. Formally, $\mu(t)$ is defined as:

$$\mu(t) = \sum_{j=0}^n c_{j,m} \mathcal{B}_{j,m}(t) \text{ s.t. } \mu(t_j) = x_{t_j}, \forall j \in \{0, \dots, n\}, \quad (19)$$

where $c_{j,m}$ is a coefficient determined by solving the linear constraints. Note that $\mu(t)$ is continuous by construction and gets increasingly smooth with the degree of the chosen bases (De Boor & De Boor, 1978). In practice, for data $x \in \mathbb{R}^d$, we calculate B-spline values at time t separately for each dimension d and concatenate them while using.

The following theorem compares the approximation error of higher-degree B-splines with that of linear interpolants.

Theorem 4.1 (Informal). *Assume $f \in \mathcal{C}^m[a, b]$ is a function with m -th bounded derivatives, and we observe its value at $n + 1$ equidistant points $\{t_j\}_{j=0}^n$. Let $\mu(t)$ be the B-spline interpolant of degree m and $p_1(t)$ be the piecewise linear interpolant that fits the observations. Then, we have $\|f(t) - \mu(t)\|_\infty = \mathcal{O}(n^{-m})$ and $\|f(t) - p_1(t)\|_\infty = \mathcal{O}(n^{-2})$.*

The degree m is chosen based on the nature of the underlying data. For nonlinear dynamical systems, the best-fit is usually greater than 2. Theorem 4.1 shows that if a function has bounded m -th derivatives, then B-spline interpolants can achieve much lower approximation error compared with linear interpolants. We provide the formal, complete version and its detailed proof in Appendix C.1. While Theorem 4.1 is stated for equidistant or regularly sampled data points, B-splines are known to be stable even in the case of irregular sampling (De Boor & De Boor, 1978; De Boor, 1976).

We conduct preliminary experiments to compare estimates obtained with B-spline and linear interpolants for trajectories sampled from a damped harmonic oscillator (see Appendix A.3 for its formal definition). Figure 1 visualizes the comparison results, where the practical implications of our theoretical results become quite clear: B-splines are much more adept at capturing the underlying curvature compared to linear interpolants. B-splines also retain the flexibility in

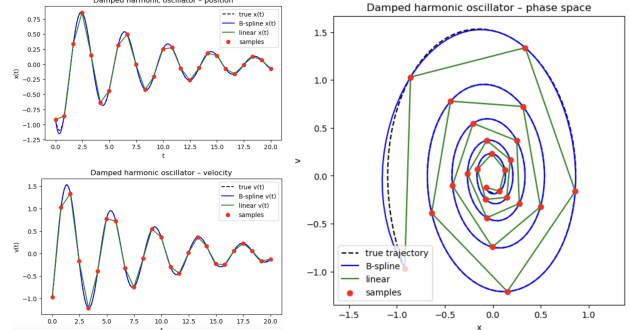


Figure 1. Visualization for interpolated trajectory sampled from a damped harmonic oscillator, which shows the performance of different interpolation methods in terms of position $x(t)$ (top-left), velocity $v(t)$ (bottom-left), and phase $(x(t), v(t))$ (right) spaces.

terms of degree with which to model, unlike cubic splines, which are restricted to the cubic degree.

Note that, for modeling dynamical systems, achieving lower function approximation error per training trajectory will ultimately lead to better approximation of the underlying first-order functional derivatives, which are used to train velocity fields in flow matching algorithms. As will be illustrated in our experiments, the use of B-spline interpolants enables the trained velocity fields to learn a more accurate structural representation of the underlying complex dynamics for both deterministic and stochastic systems, especially when the observed samples are irregularly sampled.

Theorem 4.2. *A linear interpolant is a special case of a B-spline interpolant of degree $m = 1$.*

When the underlying dynamics are actually linear in time, Theorem 4.2, proven in Appendix C.2, suggests that using B-splines can recover the performance of flow matching algorithms using linear interpolation.

4.3. Our SplineFlow Algorithm

Motivated by the efficacy, stability, and flexibility of B-splines in Section 4.2, we propose SplineFlow, which constructs conditional paths in flow matching frameworks via B-spline interpolation. Algorithm 1 details the pseudocode of SplineFlow for both deterministic and stochastic cases.

ODE Dynamics. When the underlying system dynamics are deterministic and governed by an ODE, we model the conditional probability paths $p(x | z)$ using Gaussian distributions $\mathcal{N}(x; \mu_t(z), \sigma_t^2 I)$. Different from the existing methods, we replace the $\mu_t(z)$ by B-spline interpolants defined in Equation 19 over all observations $z = (x_{t_0}, x_{t_1}, \dots, x_{t_n})$.

The following theorem proves that if we employ the above construction, we can ensure that (i) the marginal distributions can be recovered from conditional probability paths, (ii) the conditional velocity field for the dynamic case, anal-

Algorithm 1 SplineFlow

```

1: Input:  $N$  training trajectories  $\{X_i\}_{i=0}^{N-1}$ , spline degree  $m$ ,  

   learning rate  $\eta$ , base variance  $\sigma^2$ , variance, dynamics
2: Output: velocity network  $v_\theta$  and score network  $s_\phi$ 
3: Initialize parameters  $\theta$  and  $\phi$ 
4: while not converged do
5:   Sample mini-batch  $\mathcal{B} \subset \{X_i\}_{i=0}^{N-1}$ 
6:   for each  $X \in \mathcal{B}$  do
7:     Fit a B-spline interpolant of degree  $m$  to observations  

     in  $X$ , namely  $\mu(t) = \sum_j c_{j,m} \mathcal{B}_{j,m}(t)$ 
8:     Sample  $t_j \sim \mathcal{U}(t_0, t_n)$ ,  $\epsilon \sim \mathcal{N}(0, I)$ 
9:     Sample  $x_{t_j} \sim \mathcal{N}(\mu(t_j), \sigma^2(t_j)I)$ 
10:    Compute  $u(t_j) \leftarrow \mu'(t_j)$   $\triangleright$  via Theorem 4.3
11:    if variance = quadratic then
12:      Compute  $\sigma'(t_j)$   $\triangleright$  via Equation 21
13:    else
14:      Set  $\sigma'(t_j) \leftarrow 0$ 
15:    end if
16:   end for
17:   if dynamics = ODE then
18:      $\mathcal{L}(\theta) \leftarrow \frac{1}{|\mathcal{B}|} \sum_{X \in \mathcal{B}} \|v_\theta(t_j, x_{t_j}) - u(t_j)\|_2^2$ 
19:      $\theta \leftarrow \theta - \eta \nabla_\theta \mathcal{L}(\theta)$ 
20:   else  $\triangleright$  dynamics = SDE
21:      $\mathcal{L}(\theta, \phi) \leftarrow \frac{1}{|\mathcal{B}|} \sum_{X \in \mathcal{B}} (\|v_\theta(t_j, x_{t_j}) - (u(t_j) +$   

      $\epsilon \sigma'(t_j))\|_2^2 + \|\lambda(t_j) s_\phi(t_j, x_{t_j}) + \epsilon\|_2^2)$ 
22:      $\theta \leftarrow \theta - \eta \nabla_\theta \mathcal{L}(\theta, \phi)$ ,  $\phi \leftarrow \phi - \eta \nabla_\phi \mathcal{L}(\theta, \phi)$ 
23:   end if
24: end while

```

ogous to the static case as in Equation 5 satisfies the continuity equation, and (iii) the conditional velocity field that induces the B-spline probability path has an analytical form.

Theorem 4.3 (Informal). *Let $\mu_t(\cdot)$ be the B-spline interpolant of degree m defined by Equation 19 and the conditional probability path is constructed as $p_t(x | z) = \mathcal{N}(x; \mu_t(z), \sigma_t^2 I)$ with $\sigma_t(z) = \sigma \rightarrow 0$. Then, the induced marginal p_t recovers the data marginals and satisfies the continuity equation, with conditional velocity field:*

$$u_t(x | z) = \sum_{j=1}^n m c_{j,m} \left(\frac{\mathcal{B}_{j,m-1}(t)}{t_{j+m} - t_j} - \frac{\mathcal{B}_{j+1,m-1}(t)}{t_{j+m+1} - t_{j+1}} \right).$$

We present the complete, formal version of Theorem 4.3 and its proof in Appendix C.3. According to Theorem 4.3, one can show that $\nabla_\theta \mathcal{L}_{\text{CFM}} = \nabla_\theta \mathcal{L}_{\text{FM}}$ even in the dynamic case, analogous to the static case as shown in Lipman et al. (2022). This enables us to finally train the network v_θ based on the regression loss $\mathcal{L}_{\text{SplineFlow}}(\theta)$ with conditional velocity fields corresponding to a B-spline probability path. Formally, the training objective of SplineFlow is defined as:

$$\min_{\theta} \mathbb{E}_{t \sim \mathcal{U}(0,1), z \sim q(z), x \sim p_t(x | z)} \|v_\theta(t, x) - u_t(x | z)\|^2. \quad (20)$$

Once training is completed, the time-varying observations for a given initial value can be generated by integrating the velocity field: $x(t') = x(0) + \int_0^{t'} v_\theta(x_t, t) dt$ for any t' .

SDE Dynamics. When the observations X_i evolve stochastically based on Equation 9 with diffusion schedule $g(t) = \sigma$, we can write the drift $u_t(x_t)$ as in Equation 12 using the probability flow velocity field u_t^o and the probability score $\nabla_x \log(p_t(x_t))$. We know from Theorem 3.2 in Tong et al. (2023) that constructing a conditional probability flow $u_t^o(\cdot)$ and its induced probability path $p_t(\cdot)$ satisfying marginal constraints gives us a tractable way to train the probability flow velocity field approximation $v_\theta(t, x)$ and the score approximation $s_\phi(t, x)$ by optimizing over the SF2M regression loss in Equation 13. We adapt this framework to construct $p_t(x | z)$ and the induced $u_t^o(x | z)$ for modeling stochastic dynamics using SplineFlow. The following proposition, proven in Appendix C.4, states the simplified optimization objective of SplineFlow for SDE dynamics.

Proposition 4.4. *Let the underlying stochastic process have a constant diffusion σ and $p_t(x | z) = \mathcal{N}(x; \mu_t(z), \sigma_t^2(z))$ be a Spline-Bridge with B-spline mean μ_t and set $\sigma_{t_i} \rightarrow 0$ at observed timestamps. Then, for $\lambda(t) = \sigma_t(z)$, the SF2M regression objective defined in Equation 13 can be simplified as: $\mathcal{L}_{\text{SplineFlow}}(\theta, \phi) = \mathbb{E}[\|v_\theta(t, x) - (\epsilon \sigma'_t + \mu'_t)\|^2 + \|\lambda(t) s_\phi(t, x) + \epsilon\|^2]$, where $\epsilon \sim \mathcal{N}(0, I)$.*

When modeling SDE dynamics, we observed that the choice of $\sigma_t(z)$ can drastically affect performance, depending on the underlying data. Apart from a constant scheme $\sigma_t^2(z) = \sigma^2$, we also proposed a piecewise quadratic scheme:

$$\sigma_t^2(z) = \frac{\sigma^2}{(t_{j+1} - t_j)^2} (t - t_j)(t_{j+1}), \forall t \in [t_j, t_{j+1}], \quad (21)$$

which empirically works the best when modeling cellular dynamics. Algorithm 1 outlines all the necessary steps used to train the velocity network v_θ and the score network s_ϕ to obtain the SDE drift term u_t via Equation 12. Together with the diffusion schedule σ , this drift can then be integrated using the Euler-Maruyama SDE discretization scheme (Platen, 1999) to generate SDE trajectories from given initial values.

5. Experiments

Datasets. We test the performance of SplineFlow on several ODE dynamical systems, including Exponential Decay, Harmonic Oscillator, Damped Harmonic Oscillator, Lotka–Volterra, and Lorenz System, along with their SDE counterparts (see Appendix A for their definitions). In addition, we evaluate SplineFlow on the HopperPhysics dataset from the MuJoCo Physics simulation engine, and on preprocessed, log-normalized longitudinal transcriptomic datasets, including the Embryoid Body temporal data from Moon et al. (2019) and a post-traumatic brain regeneration dataset from Wei et al. (2022), across two-dimensional PHATE and PCA embeddings with 10 principal components (PCs).

Table 1. Comparisons of different methods for modeling ODE dynamics in MSE metric across 5 deterministic dynamical systems and varying sampling irregularity $p \in \{0, 0.25, 0.5, 0.75\}$. For each configuration, we highlight the best result in bold.

p	Model	Exp-Decay	Harmonic	Damped Harmonic	Lotka–Volterra	HopperPhysics	Lorenz
0	NeuralODE	0.999 ± 0.126	6.542 ± 5.965	3.474 ± 0.366	$1.98e-4 \pm 1.24e-4$	2.947 ± 0.183	1.491 ± 0.359
	LatentODE	$9.8e-5 \pm 4.7e-5$	$8.2e-4 \pm 4.2e-4$	$1.2e-4 \pm 6.3e-4$	$1.6e-3 \pm 1.2e-3$	1.894 ± 0.523	1.157 ± 0.204
	TFM	$6.6e-4 \pm 8.3e-5$	$0.181 \pm 3.8e-4$	$0.015 \pm 2.7e-4$	0.184 ± 0.104	1.554 ± 0.297	2.442 ± 0.076
	SplineFlow	$8.9e-5 \pm 3.3e-5$	$3.7e-4 \pm 3.1e-4$	$9.5e-5 \pm 1.0e-4$	0.086 ± 0.043	1.410 ± 0.172	0.639 ± 0.004
0.25	LatentODE	$9.8e-5 \pm 3.7e-5$	0.001 ± 0.001	$3.4e-4 \pm 5.8e-4$	$0.09 \pm 3.3e-4$	1.605 ± 0.019	–
	TFM	$6.9e-4 \pm 89.6e-5$	0.174 ± 0.008	$0.015 \pm 2.6e-4$	0.259 ± 0.172	1.512 ± 0.030	–
	SplineFlow	$8.2e-5 \pm 2.9e-5$	$6.5e-4 \pm 2.1e-4$	$3.0e-5 \pm 4.8e-6$	0.100 ± 0.057	1.433 ± 0.030	–
0.5	LatentODE	$1.6e-4 \pm 4.5e-5$	$7.6e-4 \pm 6.7e-5$	$7.3e-4 \pm 3.6e-4$	0.2 ± 0.001	1.649 ± 0.073	–
	TFM	$9.4e-4 \pm 1.7e-4$	0.177 ± 0.018	0.016 ± 0.001	4.259 ± 5.690	1.718 ± 0.092	–
	SplineFlow	$1.1e-4 \pm 6.8e-5$	$5.5e-4 \pm 2.2e-4$	$4.7e-5 \pm 2.1e-5$	0.705 ± 1.210	1.825 ± 0.602	–
0.75	LatentODE	$9.6e-5 \pm 5.0e-6$	$7.9e-4 \pm 2.5e-4$	$9.7e-4 \pm 3.7e-4$	0.3 ± 0.001	3.563 ± 0.148	–
	TFM	$1.4e-3 \pm 2.0e-4$	0.205 ± 0.000	0.031 ± 0.002	1.976 ± 1.810	2.810 ± 0.165	–
	SplineFlow	$8.6e-5 \pm 6.4e-6$	0.001 ± 0.001	$4.8e-5 \pm 2.3e-5$	1.783 ± 1.430	3.336 ± 0.430	–

Baselines & Metrics. We compare SplineFlow with classical adjoint-based methods, NeuralODE (Chen et al., 2018a) and LatentODE (Rubanova et al., 2019), as well as the recent simulation-free Trajectory Flow Matching (TFM) method (Zhang et al., 2024) for ODE dynamics. For SDE, we benchmark SplineFlow against the score and flow matching (SF2M) framework (Tong et al., 2023) and the classical Minibatch-OT Flow Matching (MOTFM) (Tong et al., 2024) on longitudinal transcriptomic datasets. For ODE evaluation, we compute the mean squared error (MSE) between the predicted trajectories and the ground truth. For SDE, we calculate several metrics, including the 2-Wasserstein (\mathcal{W}_2), maximum mean discrepancy (MMD), and energy distance, which measure statistical fidelity, as well as MSE on SDE and PODE (probability flow ODE) trajectories.

5.1. ODE Dynamical Systems

Table 1 demonstrates the comparison results for ODE dynamical systems, showing that SplineFlow outperforms the baselines in most settings. Compared to adjoint-based methods (Neural ODE and Latent ODE), the simulation-free methods (TFM and SplineFlow) are at least on par in terms of MSE with regularly sampled observations ($p = 0$), if not better, while being significantly faster (see detailed runtime analyses of these algorithms in Appendix D). Higher-degree interpolants in SplineFlow seem to capture the underlying dynamics much better than linear interpolants in TFM, especially in nonlinear and oscillatory systems such as Lotka–Volterra, Lorenz, and the harmonic family. Note that the Lorenz system is known to be chaotic, highly different from other dynamical systems under both deterministic ODE and stochastic SDE settings; therefore, we discuss our empirical findings separately for the Lorenz system in Section 5.3.

For irregularly sampled observations ($p > 0$), TFM with its linear interpolants performs poorly compared to SplineFlow, as observed not only from the metrics in Table 1 but also from the visualizations of the evolved dynamics in Appendix G. Higher-degree spline bases tend to better capture the underlying behavior in case of irregularity, as seen in the

degree ablations from Appendix F. While in cases where the underlying dynamics behave approximately linearly, such as in HopperPhysics, SplineFlow performs on par with TFM, since linear interpolants are a special case of B-spline interpolants with degree $m = 1$ (Theorem 4.2).

5.2. SDE Dynamical Systems

For the experiments modeling the SDE equivalents of the ODE dynamical systems with additive constant diffusion, we observed that constructing conditional probability paths with a constant variance scheme $\sigma_t^2(\mathbf{z}) = \sigma^2$ performed better than the piecewise quadratic scheme introduced in Equation 21. Table 2 summarizes the comparison results across different evaluation metrics between SplineFlow implemented with the constant scheme and the baseline SF2M. For regularly sampled observations ($p = 0$), we observe that higher-degree B-spline interpolants used to model the conditional probability paths are particularly beneficial for nonlinear (Lotka–Volterra, Lorenz) and oscillatory (damped harmonic) systems, which aligns with Theorem 4.1. For irregularly sampled observations ($p = 0.5$), SplineFlow performs better for Lotka–Volterra, whereas SF2M with its linear interpolants is the better-performing model in other cases. Due to space limit, we provide the full SDE comparison results with $p \in \{0.25, 0.5, 0.75\}$ and across other evaluation metrics in Table 33 of Appendix H.

5.3. Chaotic Dynamical Systems

Chaotic dynamical systems exhibit distinctive evolution dynamics, with drastic shifts in their states at certain time-points and highly nonlinear trajectories (Figure 2 and Figures 17–22). For Lorenz in particular, depending on the initial value, the state may converge onto one attractor basin for a period before shifting to another attractor basin, as seen in Figures 17 and 21, known as the *Butterfly Effect*. This behavior makes the system especially sensitive to masking and irregular sampling, since the state values at certain critical time points contain information about which attractor the trajectory will approach. Thus, we restrict our experiments

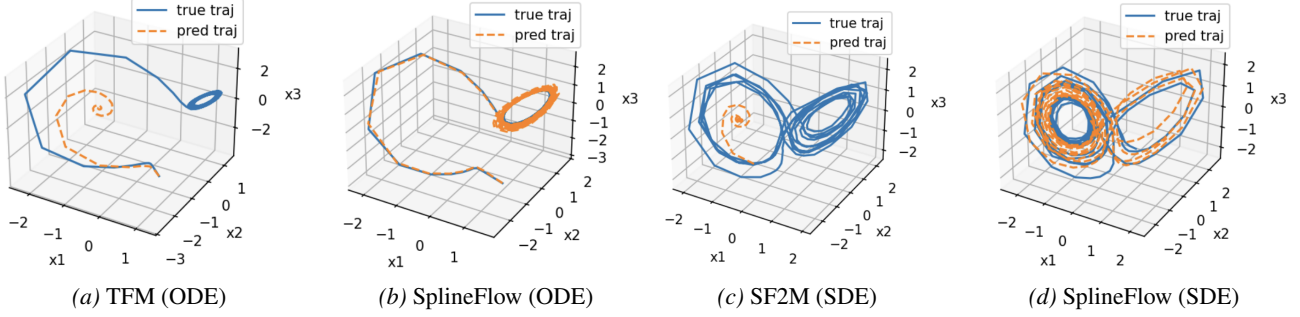


Figure 2. Visualizations of the ODE and SDE Lorenz trajectories predicted by different methods. Compared with baselines, SplineFlow learns the underlying structural properties of the Lorenz system more effectively.

Table 2. Comparisons of SplineFlow and SF2M for modeling SDE dynamics across multiple datasets and metrics, where p denotes the degree of irregularity. The best results are highlighted in bold.

Dataset	p	Model	MSE (SDE)	Wasserstein	MMD
Exp-Decay	0	SF2M	0.477 \pm 0.010	0.305 \pm 0.005	0.024 \pm 0.001
		SplineFlow	0.456 \pm 0.008	0.331 \pm 0.003	0.027 \pm 0.002
	0.5	SF2M	0.524 \pm 0.011	0.204 \pm 0.012	0.009 \pm 0.002
		SplineFlow	0.530 \pm 0.007	0.195 \pm 0.001	0.007 \pm 3.3e-4
Damped Harmonic	0	SF2M	0.967 \pm 0.033	0.430 \pm 0.007	0.048 \pm 0.003
		SplineFlow	0.970 \pm 0.008	0.410 \pm 0.004	0.042 \pm 0.002
	0.5	SF2M	0.973 \pm 0.025	0.319 \pm 0.007	0.022 \pm 0.003
		SplineFlow	0.981 \pm 0.040	0.321 \pm 0.028	0.022 \pm 0.006
Lotka–Volterra	0	SF2M	0.461 \pm 0.097	0.443 \pm 0.050	0.125 \pm 0.024
		SplineFlow	0.273 \pm 0.014	0.294 \pm 0.003	0.042 \pm 0.003
	0.5	SF2M	0.355 \pm 0.031	0.375 \pm 0.037	0.080 \pm 0.029
		SplineFlow	0.285 \pm 0.025	0.310 \pm 0.012	0.044 \pm 0.004
Lorenz	0	SF2M	2.159 \pm 0.008	0.632 \pm 0.008	0.130 \pm 0.003
		SplineFlow	1.227 \pm 0.056	0.180 \pm 0.015	0.005 \pm 0.002

on Lorenz to regular sampling ($p = 0$). In our experiments, we observe that higher-degree B-spline interpolants not only help SplineFlow outperform TFM (ODE case) and SF2M (SDE case) in terms of metric performance (Tables 1 and 2), but also enable SplineFlow to capture the underlying structure of the dynamics much better than the baselines, including the adjoint-based methods (Figures 17–22). This aligns with our theoretical motivation for using SplineFlow to model nonlinear and higher-degree dynamical systems.

5.4. Cellular Dynamics

Axolotl Brain Regeneration. We evaluate SplineFlow on a Stereo-seq spatial transcriptomics dataset (Wei et al., 2022) from a temporal study of post-traumatic brain regeneration in an Axolotl Telencephalon (Salamander) tissue. Following trauma or injury, cells undergo a complex molecular process whose underlying dynamics lead to the emergence of different cell types over time as the brain heals, making this a dynamic system of interest. The dataset contains unpaired transcriptomic expression profiles across 5 distinct stages, with replicates collected from different individual organisms at each stage. We evaluate both interpolation ($t = 3$) and extrapolation ($t = 5$) settings. For SplineFlow, we use static pairwise entropic OT couplings to generate trajectories $X_i = [x_i(1), x_i(2), x_i(3), x_i(4), x_i(5)]$ to define

Table 3. Results on transcriptomic datasets with PCA embedding.

Dataset	Task	Model	Wasserstein	MMD	Energy
Brain Regeneration	Inter.	MOTFM	0.901 \pm 0.022	0.071 \pm 0.004	1.165 \pm 0.052
		SF2M	0.888 \pm 0.007	0.067 \pm 0.001	1.144 \pm 0.012
		SplineFlow	0.838 \pm 0.014	0.058 \pm 0.003	1.019 \pm 0.039
	Extra.	MOTFM	0.799 \pm 0.003	0.135 \pm 0.007	1.652 \pm 0.043
		SF2M	0.865 \pm 0.015	0.177 \pm 0.003	1.924 \pm 0.013
		SplineFlow	0.804 \pm 0.037	0.129 \pm 0.007	1.645 \pm 0.057
Embryoid Evolution	Inter.	MOTFM	0.286 \pm 0.014	0.011 \pm 0.001	0.165 \pm 0.012
		SF2M	0.274 \pm 0.011	0.009 \pm 8.4e-04	0.155 \pm 0.013
		SplineFlow	0.296 \pm 0.015	0.013 \pm 3.1e-04	0.199 \pm 0.009
	Extra.	MOTFM	0.789 \pm 0.129	0.037 \pm 0.002	0.721 \pm 0.051
		SF2M	0.592 \pm 0.020	0.038 \pm 3.98e-04	0.747 \pm 0.012
		SplineFlow	0.539 \pm 0.034	0.036 \pm 0.004	0.689 \pm 0.101

the conditional probability paths. Since SDE modeling of cellular processes has been shown to perform better (Tong et al., 2023) than ODE modeling as used in MOTFM (Tong et al., 2024), we adopt the stochastic version of SplineFlow.

Table 3 shows that for both interpolation and extrapolation settings, SplineFlow and SF2M outperform MOTFM, highlighting the effectiveness of stochastic modeling of cellular processes. Moreover, SplineFlow outperforms SF2M, demonstrating the benefits of higher-degree B-spline interpolants. The improvement is also visible with PHATE embedding (Appendix F.4) in the interpolation setting, which is expected given that PHATE captures structural nuances in the data (Moon et al., 2019) and B-splines are better equipped than linear interpolants to model such structure.

Temporal Embryoid Evolution. Similarly, we also evaluate the unpaired transcriptomic Embryoid developmental dataset (Moon et al., 2019), spanning five developmental timepoints, in both interpolation ($t = 3$) and extrapolation ($t = 5$) settings. As in the earlier dataset, we deploy static pairwise entropic OT-couplings to generate trajectories to train a stochastic version of SplineFlow. Table 3 shows that SplineFlow consistently outperforms MOTFM and SF2M across various metrics in the extrapolation setting.

6. Conclusion

We introduced SplineFlow, a simulation-free flow matching algorithm that constructs conditional paths using B-spline

interpolants. SplineFlow provides a scalable and flexible framework for modeling complex dynamical systems, with potential applications ranging from faster data-driven simulations to modeling temporal biological processes, such as longitudinal drug treatment response. Future work may further improve upon this by learning optimal knot placement during training and by extending the framework to model stochastic dynamics with state-dependent diffusion terms.

Impact Statement

Our work contributes a general framework for data-driven modeling of dynamical systems from observational data, without requiring explicit mechanistic formulations. The proposed algorithm is particularly relevant in settings where the underlying dynamics are complex, the data are partially observed, and analytical descriptions are unavailable. The proposed framework can serve as a foundation for a range of applications, from financial market modeling to biomedical settings involving longitudinal processes, for example, analyzing biological dynamics from unpaired datasets. Future work should focus on real-world validation of model predictions in collaboration with domain experts to better assess their reliability and practical usefulness.

References

Albergo, M. S. and Vanden-Eijnden, E. Building normalizing flows with stochastic interpolants. *arXiv preprint arXiv:2209.15571*, 2022.

Arfken, G. B., Weber, H. J., and Harris, F. E. *Mathematical methods for physicists: a comprehensive guide*. Academic press, 2011.

Arnold, L. Random dynamical systems. In *Dynamical Systems: Lectures Given at the 2nd Session of the Centro Internazionale Matematico Estivo (CIME) held in Montecatini Terme, Italy, June 13–22, 1994*, pp. 1–43. Springer, 2006.

Biswas, S. and Lovell, B. C. B-splines and its applications. In *Bézier and Splines in Image Processing and Machine Vision*, pp. 109–131. Springer, 2008.

Boylestad, R. L. and Nashelsky, L. *Electronic devices and circuit theory*. Pearson, 2011.

Bunne, C., Hsieh, Y.-P., Cuturi, M., and Krause, A. The schrödinger bridge between gaussian measures has a closed form. In *International Conference on Artificial Intelligence and Statistics*, pp. 5802–5833. PMLR, 2023.

Butterfield, K. R. The computation of all the derivatives of a b-spline basis. *IMA Journal of Applied Mathematics*, 17(1):15–25, 1976.

Chen, R. T., Rubanova, Y., Bettencourt, J., and Duvenaud, D. K. Neural ordinary differential equations. *Advances in neural information processing systems*, 31, 2018a.

Chen, R. T., Rubanova, Y., Bettencourt, J., and Duvenaud, D. K. Neural ordinary differential equations. *Advances in neural information processing systems*, 31, 2018b.

De Boor, C. A bound on the l_∞ -norm of l_2 -approximation by splines in terms of a global mesh ratio. *Mathematics of computation*, 30(136):765–771, 1976.

De Boor, C. Good approximation by splines with variable knots. ii. In *Conference on the Numerical Solution of Differential Equations: Dundee 1973*, pp. 12–20. Springer, 2006.

De Boor, C. and De Boor, C. *A practical guide to splines*, volume 27. Springer New York, 1978.

De Bortoli, V., Thornton, J., Heng, J., and Doucet, A. Diffusion schrödinger bridge with applications to score-based generative modeling. *Advances in neural information processing systems*, 34:17695–17709, 2021.

Epperson, J. F. On the runge example. *The American Mathematical Monthly*, 94(4):329–341, 1987.

Gat, I., Remez, T., Shaul, N., Kreuk, F., Chen, R. T., Synnaeve, G., Adi, Y., and Lipman, Y. Discrete flow matching. *Advances in Neural Information Processing Systems*, 37:133345–133385, 2024.

Hairer, E., Wanner, G., and Nørsett, S. P. *Solving ordinary differential equations I: Nonstiff problems*. Springer, 1993.

Hasan, M. S., Alam, M. N., Fayz-Al-Asad, M., Muhammad, N., and Tunç, C. B-spline curve theory: An overview and applications in real life. *Nonlinear Engineering*, 13(1):20240054, 2024.

Karatzas, I. and Shreve, S. *Brownian motion and stochastic calculus*. Springer, 2014.

Kidger, P., Foster, J., Li, X., and Lyons, T. J. Neural sdes as infinite-dimensional gans. In *International conference on machine learning*, pp. 5453–5463. PMLR, 2021.

Léonard, C. A survey of the schrödinger problem and some of its connections with optimal transport. *arXiv preprint arXiv:1308.0215*, 2013.

Li, L. Application of cubic b-spline curve in computer-aided animation design. *Computer-Aided Design and Applications*, 18(S1):43–52, 2020.

Li, Z., Zeng, Z., Lin, X., Fang, F., Qu, Y., Xu, Z., Liu, Z., Ning, X., Wei, T., Liu, G., et al. Flow matching meets biology and life science: A survey. *arXiv preprint arXiv:2507.17731*, 2025.

Lipman, Y., Chen, R. T., Ben-Hamu, H., Nickel, M., and Le, M. Flow matching for generative modeling. *arXiv preprint arXiv:2210.02747*, 2022.

Liu, X., Gong, C., and Liu, Q. Flow straight and fast: Learning to generate and transfer data with rectified flow. *arXiv preprint arXiv:2209.03003*, 2022.

Lorenz, E. N. Deterministic nonperiodic flow 1. In *Universality in Chaos, 2nd edition*, pp. 367–378. Routledge, 2017.

Luo, X., Wang, Z., Wang, Q., Shao, X., Lv, J., Wang, L., Wang, Y., and Ma, Y. Crystalfow: a flow-based generative model for crystalline materials. *Nature Communications*, 16(1):9267, 2025.

Moon, K. R., Van Dijk, D., Wang, Z., Gigante, S., Burkhardt, D. B., Chen, W. S., Yim, K., Elzen, A. v. d., Hirn, M. J., Coifman, R. R., et al. Visualizing structure and transitions in high-dimensional biological data. *Nature biotechnology*, 37(12):1482–1492, 2019.

Nichol, A. Q. and Dhariwal, P. Improved denoising diffusion probabilistic models. In *International conference on machine learning*, pp. 8162–8171. PMLR, 2021.

Papamakarios, G., Nalisnick, E., Rezende, D. J., Mohamed, S., and Lakshminarayanan, B. Normalizing flows for probabilistic modeling and inference. *Journal of Machine Learning Research*, 22(57):1–64, 2021.

Paulsson, J. Models of stochastic gene expression. *Physics of life reviews*, 2(2):157–175, 2005.

Platen, E. An introduction to numerical methods for stochastic differential equations. *Acta numerica*, 8:197–246, 1999.

Pooladian, A.-A., Ben-Hamu, H., Domingo-Enrich, C., Amos, B., Lipman, Y., and Chen, R. T. Multisample flow matching: Straightening flows with minibatch couplings. *arXiv preprint arXiv:2304.14772*, 2023.

Rathod, S. S., Ceccarelli, F., Holden, S. B., Liò, P., Zhang, X., and Tanevski, J. Contextflow: Context-aware flow matching for trajectory inference from spatial omics data. *arXiv preprint arXiv:2510.02952*, 2025.

Rohbeck, M., De Brouwer, E., Bunne, C., Huetter, J.-C., Biton, A., Chen, K. Y., Regev, A., and Lopez, R. Modeling complex system dynamics with flow matching across time and conditions. In *The Thirteenth International Conference on Learning Representations*, 2025.

Rubanova, Y., Chen, R. T., and Duvenaud, D. K. Latent ordinary differential equations for irregularly-sampled time series. *Advances in neural information processing systems*, 32, 2019.

Schrödinger, E. Sur la théorie relativiste de l'électron et l'interprétation de la mécanique quantique. In *Annales de l'institut Henri Poincaré*, volume 2, pp. 269–310, 1932.

Schumaker, L. *Spline functions: basic theory*. Cambridge university press, 2007.

Song, Y., Sohl-Dickstein, J., Kingma, D. P., Kumar, A., Ermon, S., and Poole, B. Score-based generative modeling through stochastic differential equations. *arXiv preprint arXiv:2011.13456*, 2020.

Sørensen, H. Parametric inference for diffusion processes observed at discrete points in time: a survey. *International statistical review*, 72(3):337–354, 2004.

Tong, A., Malkin, N., Fatras, K., Atanackovic, L., Zhang, Y., Huguet, G., Wolf, G., and Bengio, Y. Simulation-free schrödinger bridges via score and flow matching. *arXiv preprint arXiv:2307.03672*, 2023.

Tong, A., FATRAS, K., Malkin, N., Huguet, G., Zhang, Y., Rector-Brooks, J., Wolf, G., and Bengio, Y. Improving and generalizing flow-based generative models with mini-batch optimal transport. *Transactions on Machine Learning Research*, 2024. ISSN 2835-8856. URL <https://openreview.net/forum?id=CD9Snc73AW>. Expert Certification.

Trefethen, L. N. *Approximation theory and approximation practice, extended edition*. SIAM, 2019.

Vargas, F., Thodoroff, P., Lamacraft, A., and Lawrence, N. Solving schrödinger bridges via maximum likelihood. *Entropy*, 23(9):1134, 2021.

Villani, C. et al. *Optimal transport: old and new*, volume 338. Springer, 2008.

Volterra, V. Variations and fluctuations of the number of individuals in animal species living together. *ICES Journal of marine science*, 3(1):3–51, 1928.

Wei, X., Fu, S., Li, H., Liu, Y., Wang, S., Feng, W., Yang, Y., Liu, X., Zeng, Y.-Y., Cheng, M., et al. Single-cell stereo-seq reveals induced progenitor cells involved in axolotl brain regeneration. *Science*, 377(6610):eabp9444, 2022.

Zhang, X. N., Pu, Y., Kawamura, Y., Loza, A., Bengio, Y., Shung, D., and Tong, A. Trajectory flow matching with applications to clinical time series modelling. *Advances in Neural Information Processing Systems*, 37:107198–107224, 2024.

Table 4. Summary of the properties of different dynamical systems considered in our experiments.

System	Linear	Non-linear	Oscillatory	Chaotic
Exponential Decay	✓	✗	✗	✗
Harmonic Oscillator	✓	✗	✓	✗
Damped Harmonic Oscillator	✓	✗	✓	✗
Lotka–Volterra	✗	✓	✓	✗
Lorenz System	✗	✓	✗	✓

A. Synthetic Dynamical Systems

We provide the formal definitions of all the synthetic dynamical systems evaluated in our experiments. Table 4 and Table 5 further summarize the properties, the corresponding ODE and SDE dynamics, and their use cases.

A.1. Exponential Decay

Exponential decay is a simple linear dynamical system, which can be written as the following ODE:

$$\dot{x}(t) = -\lambda x(t), \quad \lambda > 0. \quad (22)$$

It's often used to model first-order relaxation processes such as radioactive decay or simple stable linear systems (Arfken et al., 2011). The SDE equivalent of the exponential decay is known as an Ornstein–Uhlenbeck (OU) process given by:

$$dX_t = -\lambda X_t dt + \sigma dW_t, \quad (23)$$

where W_t denotes the standard Wiener process, λ is the hyperparameter controlling the rate of decay, and σ is the constant exogenous noise rate. OU processes are used to model systems such as the velocity of a Brownian particle under friction, gene-expression fluctuations around the steady state (Paulsson, 2005), among others.

A.2. Harmonic Oscillator

A harmonic-oscillator is bivariate dynamical system $z(t) = (x(t), v(t))$, which can be written as the following ODE:

$$\dot{x}(t) = v(t), \quad \dot{v}(t) = -\omega^2 x(t), \quad (24)$$

where W_t denotes the standard Wiener process, and ω is the natural undamped frequency of the system, and σ is the constant exogenous noise rate. It's often used to model oscillations near stable equilibria in systems, such as LC circuits (Boylestad & Nashelsky, 2011), linearized mechanical vibrations, among others.

A.3. Damped Harmonic Oscillator

A damped harmonic oscillator is a bivariate dynamical system with a damping coefficient (γ) compared to a simple harmonic oscillator above, given by the following ODE:

$$\dot{x}(t) = v(t), \quad \dot{v}(t) = -\omega^2 x(t) - 2\gamma v(t), \quad (25)$$

often used to model damped vibrations in mechanical systems with friction or RLC electronic circuits (Boylestad & Nashelsky, 2011) with resistance, among others. The stochastic equivalent is also known as a Langevin System, written as:

$$dX_t = V_t dt, \quad dV_t = (-\omega^2 X_t - 2\gamma V_t) dt + \sigma dW_t, \quad (26)$$

W_t is the standard Wiener process, and ω is the natural undamped frequency of the system, γ is the damping coefficient, and σ is the constant exogenous noise rate. It is used to model systems such as the thermal fluctuations in mechanical systems, or the motion of a Brownian particle in a quadratic potential.

A.4. Lotka–Volterra System

A Lotka–Volterra System is also known as a predator-prey dynamical system with prey populations $x(t)$ and predator populations $y(t)$, which can be written as the following ODE:

$$\dot{x}(t) = \alpha x(t) - \beta x(t)y(t), \quad \dot{y}(t) = \delta x(t)y(t) - \gamma y(t). \quad (27)$$

Table 5. Complete mathematical definition and descriptive summary of the dynamical systems considered in this work.

Dynamical System	ODE	SDE (additive noise)	Model Use Case
Exponential Decay	$\dot{x}(t) = -\lambda x(t)$	$dX_t = -\lambda X_t dt + \sigma dW_t$	First-order relaxation processes radioactive decay, simple stable linear systems mean-reverting stochastic dynamics (OU)
Harmonic	$\dot{x}(t) = v(t)$ $\dot{v}(t) = -\omega^2 x(t)$	$dX_t = V_t dt$ $dV_t = -\omega^2 X_t dt + \sigma dW_t$	Oscillations near stable equilibria LC circuits, linearized mechanical vibrations
Damped Harmonic	$\dot{x}(t) = v(t)$ $\dot{v}(t) = -\omega^2 x(t) - 2\gamma v(t)$	$dX_t = V_t dt$ $dV_t = (-\omega^2 X_t - 2\gamma V_t) dt + \sigma dW_t$	Damped mechanical vibrations RLC circuits, underdamped Langevin dynamics
Lotka–Volterra	$\dot{x}(t) = \alpha x(t) - \beta x(t)y(t)$ $\dot{y}(t) = \delta x(t)y(t) - \gamma y(t)$	$dX_t = (\alpha X_t - \beta X_t Y_t) dt + \sigma dW_t^{(1)}$ $dY_t = (\delta X_t Y_t - \gamma Y_t) dt + \sigma dW_t^{(2)}$	Predator–prey population dynamics, ecological systems chemical reaction kinetics, resource–consumer models
Lorenz	$\dot{x}(t) = \sigma(y(t) - x(t))$ $\dot{y}(t) = x(t)(\rho - z(t)) - y(t)$ $\dot{z}(t) = x(t)y(t) - \beta z(t)$	$dX_t = \sigma(Y_t - X_t) dt + \eta dW_t^{(1)}$ $dY_t = (X_t(\rho - Z_t) - Y_t) dt + \eta dW_t^{(2)}$ $dZ_t = (X_t Y_t - \beta Z_t) dt + \eta dW_t^{(3)}$	Canonical nonlinear and chaotic system sensitivity to initial conditions benchmark for learning chaotic dynamics

It is often used to model simple predator-prey population dynamics (Volterra, 1928) in ecological environments, chemical reaction kinetics, and resource-consumer models, among others. The stochastic version is used to model the influence of the outside environment in the form of perturbations, given by:

$$dX_t = (\alpha X_t - \beta X_t Y_t) dt + \sigma dW_t^{(1)}, \quad dY_t = (\delta X_t Y_t - \gamma Y_t) dt + \sigma dW_t^{(2)}, \quad (28)$$

where W_t is the standard Wiener process, α is the prey growth rate in the absence of predators, β is the rate at which predators consume prey, γ is the death rate of predators in the absence of prey to feed over, and δ is the rate at which the consumed prey converted into predator population, and σ is the constant exogenous noise rate.

A.5. Lorenz System

The Lorenz system was originally used to model simplified thermal convection dynamics in the atmosphere (Lorenz, 2017) and was shown to exhibit interesting properties, including sensitivity to initial conditions, deterministic chaotic behavior, and strange attractor patterns. It's now considered a canonical example (Arnold, 2006) in non-linear and chaotic dynamical system studies. The state evolution can be cast into an ODE as follows:

$$\dot{x}(t) = \sigma(y(t) - x(t)), \quad \dot{y}(t) = x(t)(\rho - z(t)) - y(t), \quad \dot{z}(t) = x(t)y(t) - \beta z(t). \quad (29)$$

A standard additive-noise variant is used to incorporate modeling error and exogenous influences. The stochastic Lorenz system can be written as:

$$dX_t = \sigma(Y_t - X_t) dt + \eta dW_t^{(1)}, \quad dY_t = (X_t(\rho - Z_t) - Y_t) dt + \eta dW_t^{(2)}, \quad dZ_t = (X_t Y_t - \beta Z_t) dt + \eta dW_t^{(3)}, \quad (30)$$

where $W_t^{(i)}$ are the standard Wiener processes, and (σ, ρ, β) are system-dependent model parameters controlling coupling strengths and dissipation rates, and η is the constant exogenous noise rate.

A.6. Hopper Physics (MuJoCo)

Hopper Physics is a dataset generated using the dm-control MuJoCo physics simulation library, which models the locomotion of a rigid legged system governed by gravity and rigid-body mechanics. Let $q(t)$ be generalized coordinates of the joints and $\dot{q}(t)$ be their generalized velocities. A standard form can be written as:

$$M(q)\ddot{q} + C(q, \dot{q}) + g(q) = \tau + J(q)^\top \lambda, \quad (31)$$

where M is the mass matrix, C collects Coriolis/centrifugal terms, g gravity, τ actuator torques, and $J^\top \lambda$ enforces constraints/contacts. Equivalently in first-order state $s(t) = (q(t), \dot{q}(t))$:

$$\dot{s}(t) = \begin{bmatrix} \dot{q}(t) \\ M(q)^{-1}(\tau + J(q)^\top \lambda - C(q, \dot{q}) - g(q)) \end{bmatrix}. \quad (32)$$

B. Different Kinds of Polynomial Interpolants

Let $f : [a, b] \rightarrow \mathbb{R}^d$ be an unknown function observed at samples $\{(t_i, x_i)\}_{i=0}^N$, where $x_i = f(t_i)$ and $a \leq t_0 < \dots < t_N \leq b$. An interpolation operator \mathcal{I} constructs a continuous-time function $\mathcal{I}f$ such that $(\mathcal{I}f)(t_i) = x_i$ for all i .

Linear Interpolation. A Linear Interpolant is a piecewise linear function defined as:

$$(\mathcal{I}_{\text{lin}}f)(t) = x_i \frac{t_{i+1} - t}{t_{i+1} - t_i} + x_{i+1} \frac{t - t_i}{t_{i+1} - t_i}, \quad t \in [t_i, t_{i+1}]. \quad (33)$$

It is numerically stable since it depends on local estimations. However, while the resulting interpolant is continuous, its derivatives are discontinuous at sampling points. This makes linear interpolation a suboptimal choice for modeling smooth or higher-order dynamics (Hairer et al., 1993).

Cubic Interpolation. A Cubic Interpolant $s(t)$ is a polynomial of degree three satisfying

$$s(t_i) = x_i, \quad s \in C^2([a, b]). \quad (34)$$

It's constructed so that, in addition to being a continuous function, its first two derivatives ($s'(t)$ and $s''(t)$) are also continuous, making it a popular choice for approximating smooth functions. However, the construction of $s(t)$ depends on all the sampled points (x_0, \dots, x_N) to ensure the continuity of its first two derivatives or $C^2[a, b]$ making it extremely sensitive to boundary conditions and reducing locality.

B.1. Lagrangian Interpolation

A Lagrangian Interpolant is a global polynomial defined as:

$$(\mathcal{I}_{\text{Lag}}f)(t) = \sum_{i=0}^N x_i \ell_i(t), \quad \ell_i(t) = \prod_{j \neq i} \frac{t - t_j}{t_i - t_j}. \quad (35)$$

While it is the most natural polynomial satisfying all the boundary conditions, it suffers from Runge's Phenomenon (Epperson, 1987), characterized by large oscillations and instability. Making it a poor choice to interpolate between a large number of points N . While piecewise polynomial construction can be done, it comes at the cost of discontinuous derivatives at observational time points.

B.2. Chebyshev Interpolation

Chebyshev Interpolation is polynomial interpolation at Chebyshev nodes, defined as:

$$t_k = \cos\left(\frac{(2k+1)\pi}{2(N+1)}\right), \quad (36)$$

which gives us Chebyshev Interpolants:

$$(\mathcal{I}_{\text{Cheb}}f)(t) = \sum_{k=0}^N c_k T_k(t), \quad (37)$$

where T_k are Chebyshev polynomials of the first kind, defined by $T_0(x) = 1$, $T_1(x) = x$, and $T_{k+1}(x) = 2xT_k(x) - T_{k-1}(x)$. Chebyshev Interpolation is known to improve numerical stability compared to other naïve polynomial interpolants, such as the Lagrangian Interpolant above (Trefethen, 2019). However, since the interpolant is constructed globally, it's highly unsuitable for irregularly sampled time points as is common (Trefethen, 2019).

B.3. Hermite Interpolation

A Hermitian Interpolant is a generalization of a Lagrangian Interpolant, such that apart from satisfying observational values, the derivatives at the observational points are also satisfied:

$$(\mathcal{I}_{\text{Herm}}f)(t_i) = x_i, \quad (\mathcal{I}_{\text{Herm}}f)'(t_i) = v_i. \quad (38)$$

When accurate derivative information is available, Hermitian interpolants are known to produce smooth and structurally consistent interpolations. However, the quality of the interpolant depends heavily on the availability of derivatives, which are often unavailable. Errors in derivatives lead to poorly fitted interpolants, making them a suboptimal choice (Schumaker, 2007).

B.4. B-spline Interpolation

A B-spline interpolant of degree m is defined as:

$$(\mathcal{I}_B f)(t) = \sum_k c_k B_{k,m}(t), \quad (39)$$

where $\{B_{k,m}\}$ are B-spline basis functions defined over observations via the Cox–de Boor recursion formula (Equation 18). Each basis function is locally defined, ensuring its stability, while the smoothness is controlled by the degree m . This combination of locality and smoothness control makes B-splines a particularly optimal choice for modeling dynamical functions (De Boor & De Boor, 1978).

C. Proofs of Main Theoretical Results

C.1. Proof of Theorem 4.1

Theorem 4.1 (Formal). *Let f be a function in $\mathcal{C}^m[a, b]$ with bounded m -th derivative $\|f^{(m)}\|_\infty \ll \infty$, and let $t_i = a + (i-1)h$ be $n+1$ equidistant points to be interpolated, with the distance between consecutive points being $h = \frac{b-a}{n}$. Then, assuming a well defined B-Spline interpolant with knots $\{t_i\}_{i=0}^n$, $\mu(t) = \sum_{i=0}^n c_{i,m} \mathcal{B}_{i,m}(t)$, where $\mathcal{B}_{i,m}$ is the B-Spline polynomial of degree m as defined in Equation 18, has the asymptotic function approximation error $\mathcal{O}(n^{-m})$ compared to the linear interpolant $\mathcal{O}(n^{-2})$, defined as $p_1(t) = f(t_i) + \frac{f(t_{i+1}) - f(t_i)}{t_{i+1} - t_i}(t - t_i)$ for $t \in [t_i, t_{i+1}]$.*

Or more precisely,

$$\|f(t) - \mu(t)\|_\infty \leq (1 + \|I\|) C_{m,a,b} n^{-m} \|f^{(m)}\|_\infty,$$

and

$$\|f(t) - p_1(t)\|_\infty \leq \frac{(b-a)^2}{8} \|f''\|_\infty \cdot n^{-2},$$

where $\|I\| = \sup \left\{ \frac{\|I f\|}{\|f\|} : v \in \mathcal{C}[a, b] \setminus \{0\} \right\}$ and $C_{m,a,b}$ is a constant depending only on degree m and extrema a, b .

Proof. The proof essentially boils down to combining the results from Corollary C.2 and Lemma C.4 containing the function approximation error rates for the linear interpolant $p_1(t)$ and B-Spline interpolant $\mu(t)$.

From Corollary C.2 we can write,

$$\|f(t) - p_1(t)\|_\infty \leq \frac{1}{8} \Delta_{\max}^2 |f''(t)|_\infty. \quad (40)$$

Here, $\Delta_i = t_{i+1} - t_i$ and $\Delta_{\max} = \max_i \Delta_i$, and for equidistant points, $\Delta_{\max} = \frac{b-a}{n}$ which after substituting in the above Equation 40 gives us the required result for linear interpolation:

$$\|f(t) - p_1(t)\|_\infty \leq \frac{(b-a)^2}{8} \|f''\|_\infty \cdot (n)^{-2}, \quad (41)$$

Similarly, knowing that $\Delta_{\max} = \frac{b-a}{n}$ for equidistant points and utilizing result from Lemma C.1 gives us,

$$\|f(t) - \mu(t)\|_\infty \leq (1 + \|I\|) C_{m,a,b} n^{-m} \|f^{(m)}\|_\infty. \quad (42)$$

From Equations 41 and 42, we get the required result. \square

C.2. Proof of Theorem 4.2

Theorem 4.2 (Formal). Let $\mu(t)$ be a well defined B-Spline interpolant, interpolating function $f(t) \in \mathcal{C}^2[a, b]$ with observation sites at $\{\tau_i\}_{i=0}^n$, $\mu(t) = \sum_{i=0}^n c_{i,m} \mathcal{B}_{i,m}(t)$, where $\mathcal{B}_{i,m}$ is the B-Spline polynomial of degree m as defined in Equation 18. Then, degree 1 interpolant or μ_t with $m = 1$ is equivalent to the linear interpolant defined as $p_1(t) = f(t_i) + \frac{f(t_{i+1}) - f(t_i)}{t_{i+1} - t_i}(t - t_i)$ for any $t \in [t_i, t_{i+1}]$.

Proof. We clamp the observation sites to get $n + 3$ knots: $\tau_0 = \tau_1 < \tau_2 \cdots \tau_n < \tau_{n+1} = \tau_{n+2}$ with $\tau_0 = \tau_1 = t_0$, $\tau_{n+1} = \tau_{n+2} = t_n$, and $\tau_i = t_{i-1}$ for $i \in [1, n + 1]$.

From the definition of B-Splines in earlier section 4.2 we know that the 0-th degree B-Spline basis is defined as:

$$\mathcal{B}_{i,0} = \begin{cases} 1 & \text{if } t \in [\tau_i, \tau_{i+1}), \\ 0 & \text{otherwise.} \end{cases} \quad (43)$$

With the higher degree B-Spline basis defined recursively as:

$$\mathcal{B}_{i,m}(t) = \frac{t - \tau_i}{\tau_{i+m} - \tau_i} \mathcal{B}_{i,m-1}(t) + \frac{\tau_{i+m+1} - t}{\tau_{i+m+1} - \tau_{i+1}} \mathcal{B}_{i+1,m-1}(t). \quad (44)$$

The interpolant function $\mu(t)$ of degree m is then a linear combination of B-Splines around $n + 3$ knots, written as:

$$\mu(t) = \sum_{i=0}^{n+2} c_{i,m} \mathcal{B}_{i,m}(t) \quad \text{s.t.} \quad \mu(t_0) = f(t_0), \mu(t_1) = f(t_1), \dots, \mu(t_n) = f(t_n). \quad (45)$$

Since our degree $m = 1$, we thus focus on getting expressions for $\mathcal{B}_{i,1}$, starting with the left and right endpoints.

From Cox-De Boor recursion from Equation 44 we know that,

$$\mathcal{B}_{0,1}(t) = \frac{t - \tau_0}{\tau_1 - \tau_0} \mathcal{B}_{0,0}(t) + \frac{\tau_2 - t}{\tau_2 - \tau_1} \mathcal{B}_{1,0}(t).$$

Since $\tau_0 = \tau_1 = t_0$ we have that $\mathcal{B}_{0,0} \equiv 0$, so we get that $\mathcal{B}_{0,1}(t) = \frac{t_1 - t}{t_1 - t_0} \mathcal{B}_{1,0}$, which gives us,

$$\mathcal{B}_{0,1}(t) = \begin{cases} \frac{t_1 - t}{t_1 - t_0}, & t \in [t_0, t_1), \\ 0, & \text{otherwise.} \end{cases} \quad (46)$$

Similarly for the right endpoint, we have that $\tau_{n+1} = \tau_{n+2} = t_{n+1}$ which implies $\mathcal{B}_{n+2,0} \equiv 0$. And using this in the Cox-De Boor recursion formula (Equation 44) gives us,

$$\mathcal{B}_{n+2,1}(t) = \begin{cases} \frac{t - t_n}{t_{n+1} - t_n}, & t \in [t_{n-1}, t_n], \\ 0, & \text{otherwise.} \end{cases} \quad (47)$$

For $i \in [1, n + 1]$ we have that

$$\mathcal{B}_{i,1}(t) = \frac{t - \tau_i}{\tau_{i+1} - \tau_i} \mathcal{B}_{i,0}(t) + \frac{\tau_{i+2} - t}{\tau_{i+2} - \tau_{i+1}} \mathcal{B}_{i+1,0}(t), \quad (48)$$

and from Equation 43 we know that $\mathcal{B}_{i,0}(t) = 1$ in $t \in [\tau_i, \tau_{i+1})$, $\mathcal{B}_{i+1,0}(t) = 1$ in $t \in [\tau_{i+1}, \tau_{i+2})$, and utilizing the fact that $\tau_i = t_{i-1}$ for $i \in [1, n + 1]$, gives us

$$\mathcal{B}_{i,1}(t) = \begin{cases} \frac{t - t_{i-1}}{\tau_i - t_{i-1}}, & t \in [t_{i-1}, t_i) \\ \frac{t_{i+1} - t}{\tau_{i+1} - t_i}, & t \in [t_i, t_{i+1}) \\ 0 & \text{otherwise.} \end{cases} \quad (49)$$

We can now use the constraints from Equation 45 and Equations 46, 49, 47 to solve and get,

$$c_{0,1} = c_{1,1} = f(t_0), c_{2,1} = f(t_1), \dots, c_{n,1} = f(t_{n-1}), c_{n+1,1} = c_{n+2,1} = f(t_n) \quad (50)$$

Finally, to prove the equivalence with the linear interpolant, consider the B-Spline interpolant $\mu(t)$ for $t \in [t_i, t_{i+1}]$. We know that,

$$\mu(t) = \sum_{i=0}^{n+2} c_{i,m} \mathcal{B}_{i,m}(t).$$

Utilizing Equations 49 and 50, we get that

$$\begin{aligned} \mu(t) &= f(t_i) \frac{t_{i+1} - t}{t_{i+1} - t_i} + f(t_{i+1}) \frac{t - t_i}{t_{i+1} - t_i} \\ &= \frac{f(t_i)(t_{i+1} - t_i) + f(t_i)t_i - f(t_{i+1})t_i + t(f(t_{i+1}) - f(t_i))}{t_{i+1} - t_i} \\ &= f(t_i) + \frac{f(t_{i+1}) - f(t_i)}{t_{i+1} - t_i} \times (t - t_i), \end{aligned}$$

which gives

$$\mu(t) = p_1(t) = f(t_i) + \frac{f(t_{i+1}) - f(t_i)}{t_{i+1} - t_i} \times (t - t_i).$$

Thus, we have proven the equivalence between degree $m = 1$ B-Spline interpolant and linear interpolant $p_1(t)$. \square

C.3. Proof of Theorem 4.3

Theorem 4.3 (Formal). *Let $\mu(t)$ be the degree m B-Spline interpolant for trajectories $X = [x_{t_0}, x_{t_1}, \dots, x_{t_n}]$ as defined in Equation 18, and let the latent be $z = (x_{t_0}, x_{t_1}, \dots, x_{t_n})$ with the distribution $q(z)$ over observed trajectories. Then, choosing the conditional probability path as $p_t(x|z) = \mathcal{N}(x; \mu_t(z), \sigma_t^2(z))$ with $\sigma_t(z) = \sigma \rightarrow 0$, enables the following:*

- The marginal probability distribution written as, $p_t(x) = \int p_t(x|z)q(z)dz$ satisfies the observation distribution with $p_{t=t_i}(x) = q(x_{t_i} = x)$.
- The marginal velocity field written as $u_t(x) = \int u_t(x | z) \frac{p_t(x|z)q(z)}{p_t(x)} dz$ and the marginal probability $p_t(\cdot)$ obey the continuity equation $\frac{\partial p_t(x)}{\partial t} = -\nabla \cdot (u_t(x)p_t(x))$.
- The conditional probability path defined above is generated by the conditional velocity field given by $u_t(x | z) = \sum_{i=1}^n m \times c_{i,m} \left\{ \frac{\mathcal{B}_{i,m-1}(t)}{t_{i+m} - t_i} - \frac{\mathcal{B}_{i+1,m-1}(t)}{t_{i+m+1} - t_{i+1}} \right\}$.

Proof. (A). We know that $\lim_{\sigma \rightarrow 0} \mathcal{N}(x; \mu(t | z), \sigma^2 I) = \delta(x - \mu(t | z))$, where δ is the delta distribution. For $t = t_i$ we can thus write

$$p_{t=t_i}(x) = \int \delta(x - \mu(t_i | z))q(z)dz.$$

Since $\mu(\cdot)$ is a B-Spline interpolant, we have that $\mu(t_i | z) = x_{t_i}$. Thus, we have

$$\begin{aligned} p_{t=t_i}(x) &= \int \delta(x - x_{t_i})q(z)dz \\ &= \int \dots \int \delta(x - x_{t_i})q(x_{t_0}, x_{t_1}, \dots, x_{t_n})dx_{t_0} \dots dx_{t_n} \\ &= \int \delta(x - x_{t_i}) \left(\int \dots \int q(x_{t_0}, x_{t_1}, \dots, x_{t_n})dx_{t_0} \dots dx_{t_n} \right) dx_{t_i} \\ &= \int \delta(x - x_{t_i})q(x_{t_i})dx_{t_i} \\ &= q(x = x_{t_i}), \end{aligned}$$

which gives us the required result.

(B). This result follows from a simple extension of Theorem 1 from [Lipman et al. \(2022\)](#). We can write the marginal p_t as $p_t(x) = \int p_t(x|z) q(z) dz$, which gives us

$$\frac{\partial p_t(x)}{\partial t} = \frac{\partial}{\partial t} \int p_t(x|z) q(z) dz.$$

Invoking Continuity Equation (from Equation 2) for the conditional probability, we get

$$\begin{aligned} \frac{\partial p_t(x)}{\partial t} &= \int -\nabla \cdot (u_t(x|z) p_t(x|z)) q(z) dz \\ &= \int -\nabla \cdot (u_t(x|z) p_t(x|z) q(z)) dz \\ &= -\nabla \cdot \int u_t(x|z) \frac{p_t(x|z) q(z)}{p_t(x)} p_t(x) dz \\ &= -\nabla \cdot \left(\int u_t(x|z) \frac{p_t(x|z) p(z)}{p_t(x)} dz \right) p_t(x) \\ &= -\nabla \cdot \left(\int u_t(x|z) \frac{p_t(x|z) q(z)}{p_t(x)} dz \right) p_t(x). \end{aligned}$$

Utilizing the fact that the marginal velocity can be written as $u_t(x) = \int u_t(x|z) \frac{p_t(x|z) q(z)}{p_t(x)} dz$ we get the required result:

$$\frac{\partial p_t(x)}{\partial t} = -\nabla \cdot (u_t(x) p_t(x)).$$

(C). The random variable $x \sim \mathcal{N}(x; \mu_t(z), \sigma^2 I)$ can be written as

$$x_t = \mu_t(z) + \sigma \epsilon, \quad \epsilon \sim \mathcal{N}(0, 1).$$

Then, from Equation 8 or Theorem 3 from [Lipman et al. \(2022\)](#) we get that

$$u_t(x|z) = \frac{\sigma'_t(z)}{\sigma_t(z)} (x - \mu_t(z)) + \mu'_t(z) = 0 + \frac{d\mu_t(z)}{dt},$$

where the last equality follows from the fact that σ is constant. Utilizing the result from Lemma C.5, we obtain

$$u_t(x|z) = \sum_{i=1}^n m \times c_{i,m} \left\{ \frac{\mathcal{B}_{i,m-1}(t)}{t_{i+m} - t_i} - \frac{\mathcal{B}_{i+1,m-1}(t)}{t_{i+m+1} - t_{i+1}} \right\},$$

which completes the proof. \square

C.4. Proof of Proposition 4.4

Proposition 4.4 (Formal). *Let the trajectories $X = [x_{t_0}, x_{t_1}, \dots, x_{t_n}]$ be observations from the SDE dynamics as defined in Equation 9, with constant diffusion term $g(t) = \sigma$, and let the latent be $z = (x_{t_0}, x_{t_1}, \dots, x_{t_n})$ with the distribution $q(z)$ over observed trajectories. Then, choosing the conditional probability path as a Spline-Bridge $p_t(x|z) = \mathcal{N}(x; \mu_t(z), \sigma_t^2(z))$ with $\lim_{\sigma(t_i; z) \rightarrow 0}$, where $\mu_t(z)$ is the B-spline interpolant and setting the time conditional weights $\lambda(t) = \sigma_t(z)$ we can write the regression loss $\mathcal{L}_{\text{SplineFlow}}$ as:*

$$\mathcal{L}_{\text{SplineFlow}}(\theta, \phi) = \mathbb{E}_{t,z,x} \left[\|v_\theta(t, x) - (\epsilon \sigma'_t(z) + \mu'_t(z))\|^2 + \|\lambda(t) s_\phi(t, x) + \epsilon\|^2 \right],$$

where $\epsilon \sim \mathcal{N}(0, 1)$ and the expectation is defined over time $t \sim \mathcal{U}(0, 1)$, the latent variables $z \sim q(z)$ and the conditional probability samples $x \sim p_t(x|z)$.

Proof. We know from the preliminaries (Section 3) that for a given diffusion $g(t)$ the SDE dynamics can be recovered by approximating the drift ($u_t(\cdot)$) by utilizing the probability flow velocity field $u_t^o(\cdot)$ and the probability score ($\nabla_t p(\cdot)$). The regression loss from Score and Flow Matching objective (Tong et al., 2023) can thus be written as:

$$\mathcal{L}_{[\text{SF}]^2\text{M}}(\theta, \phi) = \mathbb{E}_{t,z,x} \left[\|v_\theta(t, x) - u_t^o(x|z)\|^2 + \lambda(t)^2 \|s_\phi(t, x) - \nabla \log p_t(x|z)\|^2 \right]. \quad (51)$$

And as shown in Lipman et al. (2022) for conditional gaussian paths $p_t(x|z) = \mathcal{N}(x|\mu_t(z), \sigma_t(z)^2)$, the velocity field inducing the distribution can be written as

$$u_t^o(x|z) = \frac{\sigma'_t(z)}{\sigma_t(z)}(x - \mu_t(z)) + \mu'_t(z). \quad (52)$$

The samples from the conditional probability path $p_t(x|z) = \mathcal{N}(x|\mu_t(z), \sigma_t^2(z))$ can be written as:

$$x_t = \mu_t(z) + \epsilon \sigma_t(z).$$

After substitution in Equation 52, we have

$$u_t^o(x|z) = \sigma'_t(z)\epsilon + \mu'_t(z). \quad (53)$$

And since x_t is a gaussian random variable, we get

$$\nabla_x p(x|z) = -\frac{(x - \mu_t(z))}{\sigma_t^2(z)},$$

which after using the fact that $x_t = \mu_t(z) + \epsilon \sigma_t(z)$ gives us

$$\nabla_x p(x|z) = -\frac{\epsilon}{\sigma_t(z)}. \quad (54)$$

Substituting Equation 54, Equation 53, and the given $\lambda(t) = \sigma_t(z)$ into the regression loss in Equation 51 gives us the required result,

$$\mathcal{L}_{\text{SplineFlow}}(\theta, \phi) = \mathbb{E}_{t,z,x} \left[\|v_\theta(t, x) - (\epsilon \sigma'_t(z) + \mu'_t(z))\|^2 + \|\lambda(t)s_\phi(t, x) + \epsilon\|^2 \right].$$

□

C.5. Technical Lemmas used for Proving Main Theorems

Lemma C.1. *Let $f(t)$ be a continuous and twice differentiable function in $\mathcal{C}^2[t_i, t_{i+1}]$, with $t_i, t_{i+1} \in \mathbb{R}$, then $\exists \xi \in [t_i, t_{i+1}]$ s.t.*

$$f(t) = f(t_i) + \left(\frac{f(t_{i+1}) - f(t_i)}{t_{i+1} - t_i} \right)(t - t_i) + \frac{f''(\xi)}{2}(t - t_i)(t - t_{i+1}).$$

Proof. Define the linear interpolant as

$$p_1(t) := f(t_i) + \frac{f(t_{i+1}) - f(t_i)}{t_{i+1} - t_i}(t - t_i). \quad (55)$$

Consider some intermediary functions as

$$L(t) := f(t) - p_1(t), \quad \phi(t) := (t - t_i)(t - t_{i+1}). \quad (56)$$

For a fixed $x \in (t_i, t_{i+1})$, define the auxiliary function as

$$g(y) := L(y) - \frac{L(t)}{\phi(t)} \phi(y), \quad y \in [t_i, t_{i+1}].$$

We observe that

$$g(t_i) = g(t_{i+1}) = g(t) = 0.$$

Thus by Mean Value Theorem we know that, $\exists \xi_1 \in (t_i, x)$ and $\exists \xi_2 \in (t, t_{i+1})$ such that

$$g'(\xi_1) = g'(\xi_2) = 0.$$

Applying Mean Value Theorem theorem again, we get that $\exists \xi \in (t_i, t_{i+1})$ such that

$$g''(\xi) = 0.$$

Since $p_1(t)$ is linear, $p_1''(t) = 0$, and $\phi''(y) = 2$. We thus get

$$\begin{aligned} g''(y) &= f''(y) - 2 \frac{L(t)}{\phi(t)}, \\ \implies f''(\xi) - \frac{2L(t)}{\phi(t)} &= 0 \\ \implies L(t) &= \frac{f''(\xi)\phi(t)}{2} \\ \implies L(t) &= \frac{f''(\xi)}{2}(t - t_i)(t - t_{i+1}). \end{aligned}$$

Using this and Equations 55 and 56, we get

$$f(t) = p_1(t) + \frac{f''(\xi)}{2}(t - t_i)(t - t_{i+1}), \quad \xi \in (t_i, t_{i+1}),$$

which completes the proof. \square

Corollary C.2. *Let $f(t)$ be a continuous and twice differentiable function in $C^2[a, b]$, sampled at timepoints $\{t_0, t_1, \dots, t_n\}$ such that $a < t_0 < t_1 \dots < t_n < b$ with $p_1(t) = f(t_i) + \frac{f(t_{i+1}) - f(t_i)}{t_{i+1} - t_i}(t - t_i)$ be the linear interpolant in the interval $[t_i, t_{i+1}]$. Then, the approximation error is given by the following inequality:*

$$\|f(t) - p_1(t)\|_\infty \leq \frac{1}{8} \Delta_{\max}^2 |f''(t)|_\infty,$$

where $\Delta_i = t_{i+1} - t_i$ and $\Delta_{\max} = \max_i \Delta_i$.

Proof. From Theorem C.1 we know that for $t \in [t_i, t_{i+1}]$, $\exists \xi \in [t_i, t_{i+1}]$ such that $f(t)$ could be written as

$$f(t) = f(t_i) + \left(\frac{f(t_{i+1}) - f(t_i)}{t_{i+1} - t_i} \right)(t - t_i) + \frac{f''(\xi)}{2}(t - t_i)(t - t_{i+1}),$$

which could be rewritten as

$$f(t) = p_1(t) + \frac{f''(\xi)}{2}(t - t_i)(t - t_{i+1}).$$

The approximation error then becomes

$$f(t) - p_1(t) = \frac{f''(\xi)}{2}(t - t_i)(t - t_{i+1}), \quad \|f(t) - p_1(t)\|_\infty \leq \frac{f''(\xi)}{8}(t_{i+1} - t_i)^2.$$

Taking a supremum over all the intervals gives us the required bound

$$\|f(t) - p_1(t)\|_\infty \leq \Delta_{\max}^2 \frac{\|f''(t)\|_\infty}{8}.$$

\square

Lemma C.3. Let $t = (t_i)_{i=1}^{n+k}$ be a knot sequence with $t_1 = \dots = t_k = a < \dots < b = t_{n+1} = \dots = t_{n+k}$ and mesh size $\Delta_{\max} := \max_i(t_{i+1} - t_i)$. Let $S_{k,t}$ denote the spline space of degree k with knots t . Assume that the interpolation operator $I : C([a,b]) \rightarrow S_{k,t}$ is well-defined and bounded, with interpolation sites at $\tau_0 < \tau_1 < \dots < \tau_n$ for $g \in C^k([a,b])$, such that $Ig(\tau_i) = g(\tau_i)$. Then there exists a constant $C_k > 0$, depending only on k , such that

$$\|g - Ig\|_\infty \leq (1 + \|I\|) C_k \Delta_{\max}^k \|g^{(k)}\|_\infty.$$

Proof. We know that the interpolant operator I is linear, and for any $s \in S_{k,t}$ since the interpolant is well defined by assumption we get that $Is = s$. We can thus write

$$g - Ig = (g - s) - I(g - s).$$

Hence, we get

$$\|g - Ig\|_\infty \leq \|g - s\|_\infty + \|I(g - s)\|_\infty \leq (1 + \|I\|) \|g - s\|_\infty.$$

Taking the infimum over $s \in S_{k,t}$ yields

$$\|g - Ig\|_\infty \leq (1 + \|I\|) \text{dist}(g, S_{k,t}).$$

From Lemma C.4 we know that, if $g \in C^k([a,b])$ then $\text{dist}(g, S_{k,t}) \leq C_k \Delta_{\max}^k \|g^{(k)}\|_\infty$. Combining the two inequalities proves the result. \square

Lemma C.4. Let $t = (t_i)_{i=1}^{n+k}$ satisfy $t_1 = \dots = t_k = a < \dots < b = t_{n+1} = \dots = t_{n+k}$ and let $\Delta_{\max} := \max_i(t_{i+1} - t_i)$. Let $S_{k,t}$ be the spline space of degree k (degree $\leq k-1$) with knots t , and define

$$\text{dist}(g, S_{k,t}) := \inf_{s \in S_{k,t}} \|g - s\|_\infty.$$

If $g \in C^k([a,b])$, then there exists a constant C_k (depending only on k) such that

$$\text{dist}(g, S_{k,t}) \leq C_k \Delta_{\max}^k \|g^{(k)}\|_\infty.$$

Proof. Refer to Chapter 12 from (De Boor & De Boor, 1978) or (De Boor, 2006) for the detailed proof. \square

Lemma C.5. Let $\mu(t)$ be a well defined B-Spline interpolant, interpolating function $f(t) \in C^m[a,b]$ with observation sites at $\{t_i\}_{i=0}^n$, $\mu(t) = \sum_{i=0}^n c_{i,m} \mathcal{B}_{i,m}(t)$, where $\mathcal{B}_{i,m}$ is the B-Spline polynomial of degree m as defined in Equation 18. Then, the derivative of the interpolant function can be written as:

$$\frac{d\mu(t)}{dt} = \sum_{i=1}^n m \times c_{i,m} \left\{ \frac{\mathcal{B}_{i,m-1}(t)}{t_{i+m} - t_i} - \frac{\mathcal{B}_{i+1,m-1}(t)}{t_{i+m+1} - t_{i+1}} \right\}.$$

Proof. The result follows from the following classical result in spline theory which says that let

$$\mathcal{B}_{i,0} = \begin{cases} 1 & \text{if } t \in [t_i, t_{i+1}), \\ 0 & \text{otherwise.} \end{cases}$$

With higher degree B-Spline basis defined as:

$$\mathcal{B}_{i,m}(t) = \frac{t - t_i}{t_{i+m} - t_i} \mathcal{B}_{i,m-1}(t) + \frac{t_{i+m+1} - t}{t_{i+m+1} - t_{i+1}} \mathcal{B}_{i+1,m-1}(t).$$

Then, the derivative of $\mathcal{B}_{i,m}$ is given by

$$\frac{d\mathcal{B}_{i,m}(t)}{dt} = m \times \left\{ \frac{\mathcal{B}_{i,m-1}(t)}{t_{i+m} - t_i} - \frac{\mathcal{B}_{i+1,m-1}(t)}{t_{i+m+1} - t_{i+1}} \right\}. \quad (57)$$

This is classical result from Butterfield (1976) also present in De Boor & De Boor (1978) that can be derived using the method of divided differences. We can thus write

$$\frac{d\mu(t)}{dt} = \sum_i c_{i,m} \frac{d\mathcal{B}_{i,m}(t)}{dt}.$$

Utilizing Equation 57, the result follows. \square

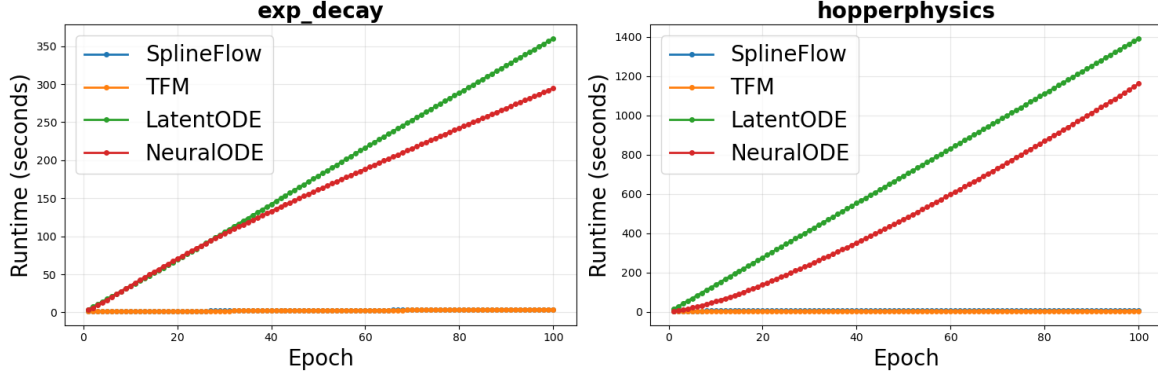


Figure 3. Runtime comparison between adjoint ODE-based and simulation-free flow matching methods for Exponential Decay ($d = 1$) and HopperPhysics ($d = 14$).

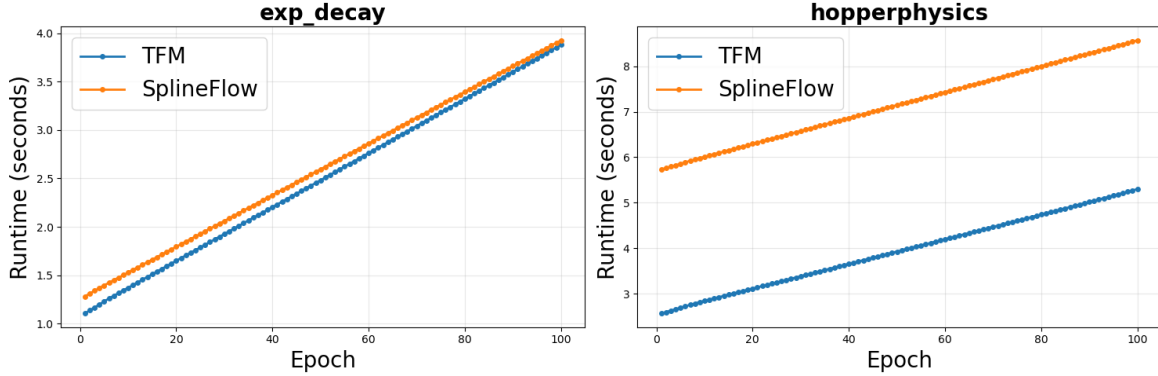


Figure 4. Runtime comparison between flow matching methods for Exponential Decay ($d = 1$) and HopperPhysics ($d = 14$).

D. Runtime Comparison

While using SplineFlow, the total runtime depends on (a) creating B-splines, (b) sampling values and derivatives from B-splines, and (c) forward-backward passes for each epoch. Consider a total of N trajectories of dimensionality D , each with n observations in total, interpolated with B-splines of order m , and let Q be the number of sampling queries made to calculate conditional velocities and values. Let total epochs be T and let F be the average time taken for each forward-backward pass while training on the regression objective for a batch size B .

Complexity for B-spline construction. For every trajectory, for each observation i we need to recursively create m spline bases, and each interval $t \in [t_i, t_{i+1}]$, we have m bases from neighbouring observations to add. And since we do this separately for each dimension D , the cost comes out as $\mathcal{O}(NDnm^2)$.

Complexity for sampling from B-splines. For every Q queries we evaluate from the B-spline construction (for conditional entities), for every trajectory, we again sum over m bases for each query, thus bringing the cost to $\mathcal{O}(2 \times NQDm)$, together for x_t and v_t .

Total Time Complexity. The complexity for calculating precomputed conditional paths and velocities is thus $\mathcal{O}(NDm(nm + Q))$. These precomputed entities are then passed along the training algorithm, with a total time of $\mathcal{O}(TF)$ per batch B and N/B dataloader passes per epoch. Thus the total complexity comes out to be $\mathcal{O}(NDm(nm + Q) + TF \times (N/B))$.

We also ran runtime experiments with baselines and SplineFlow ($m = 3$) on the smallest-dimensional Exponential Decay dataset ($d = 1$) and the largest-dimensional HopperPhysics dataset ($d = 14$) for comparison. Figure 3 demonstrates significant advantages of simulation-free methods in terms of total runtime. LatentODE, owing to its encoder-decoder architecture, has a higher runtime than NeuralODE. Whereas from Figure 4, we can see that for Exponential Decay $d = 1$, both TFM and SplineFlow have almost identical runtime. For HopperPhysics, SplineFlow incurs about 3 seconds of B-spline calculation overhead compared to the linear-interpolant calculation, as shown in Table 6 below. However, it's important to note that this overhead is a one-time cost incurred before training begins and thus doesn't affect the overall training time.

Table 6. Time taken for processing of conditional paths and velocities before training epochs begin

Dataset	Method	Time (s)
Exponential Decay	SplineFlow	1.116
	TFM	0.934
HopperPhysics	SplineFlow	5.558
	TFM	2.407

E. Hyperparameter Selection

Degree of B-Spline Interpolant m . The degree m could be selected by performing a simple cross-validation on training data. Let $\{X^i\}_{i \in [1 \dots N]}$ be observed trajectories as defined in Section 4. For each trajectory X^i create a fit X_{fit}^i and test X_{test}^i subsets such that $X_{\text{fit}}^i \cup X_{\text{test}}^i = X^i$. Fit a B-spline interpolant as defined in Equation 19 (\mathcal{I}_m) of degree m such that the interpolant satisfies observations at fit subset $\mathcal{I}_m(X_{\text{fit}}^i) = X_{\text{fit}}^i$, and calculate the error on X_{test}^i as $\sum_{i \in \text{training}} \|\mathcal{I}_m(X_{\text{test}}^i) - X_{\text{test}}^i\|^2$. Then, we can select the degree that minimizes the error.

Constant Diffusion Schedule σ . Consider trajectory X^i , $i \in \{1, \dots, N\}$, sampled from the SDE evolution with constant diffusion schedule mentioned in Equation 9: $dx_t = u_t(x_t)dt + \sigma dw_t$, with $x \in \mathbb{R}^d$. Let trajectory i contain n_i observations $\{x_i(t_0^i), \dots, x_i(t_{n_i}^i)\}$, then the constant diffusion term σ can then be estimated using a discrete estimator below:

$$\hat{\sigma}^2 = \frac{1}{d \sum_{i=1}^N T_i} \sum_{i=1}^N \sum_{k=0}^{n_i-1} \|x_i(t_{k+1}^i) - x_i(t_k^i)\|_2^2, \quad (58)$$

where $T_i = \sum_{k=1}^{n_i} (t_{k+1} - t_k)$ is the sum of time differences.

This estimator follows from classical results on quadratic variation of Ito diffusions, which imply that the sum of squared increments converges to the integrated diffusion coefficient (Sørensen, 2004; Karatzas & Shreve, 2014). Note that the estimator is meant to provide a guide for selecting the hyperparameter σ ; however, the input (σ) to Algorithm 1 should still be at the discretion of the user.

F. Additional Experiments and Ablations

F.1. ODE Dynamics (ablations with order k) for non-linear and oscillatory systems

From the ablation study in this section, we observe that higher degree B-splines are the most useful when modeling at high irregularity ($p > 0$) regimes, for example, Damped Harmonic and Lotka–Volterra. For systems with linear dynamics, like HopperPhysics, linear degree performs best.

F.1.1. DAMPED HARMONIC OSCILLATOR

 Table 7. Effect of spline degree on MSE performance of SplineFlow on damped harmonic system across missingness probabilities p .

Degree	$p = 0$	$p = 0.25$	$p = 0.5$	$p = 0.75$
1	$1.97e-2 \pm 4.83e-4$	$2.05e-2 \pm 2.69e-3$	$3.19e-2 \pm 4.18e-3$	$1.71e-1 \pm 3.71e-2$
2	$6.5e-5 \pm 3.47e-5$	$6.2e-5 \pm 2.69e-5$	$5.4e-5 \pm 3.44e-5$	$4.15e-4 \pm 8.13e-5$
3	$3.1e-5 \pm 8.47e-6$	$2.9e-5 \pm 9.69e-6$	$1.00e-4 \pm 8.68e-5$	$1.84e-4 \pm 4.29e-5$
4	$7.2e-5 \pm 3.02e-5$	$5.1e-5 \pm 3.44e-5$	$4.7e-5 \pm 3.37e-5$	$3.4e-5 \pm 4.54e-6$
5	$9.5e-5 \pm 1.02e-4$	$3.0e-5 \pm 4.77e-6$	$4.7e-5 \pm 2.14e-5$	$4.8e-5 \pm 2.30e-5$

F.1.2. LOTKA–VOLTERRA

 Table 8. Effect of spline degree on MSE performance of SplineFlow on Lotka–Volterra system across missingness probabilities p .

Degree	$p = 0$	$p = 0.25$	$p = 0.5$	$p = 0.75$
1	$4.19e+0 \pm 7.51e+0$	$4.29e+0 \pm 6.00e+0$	$1.22e+1 \pm 8.84e+0$	$2.15e+2 \pm 1.28e+2$
2	$5.83e-2 \pm 4.14e-2$	$2.56e-1 \pm 2.05e-1$	$3.56e-1 \pm 2.24e-1$	$6.82e+0 \pm 3.98e+0$
3	$4.50e-2 \pm 2.78e-2$	$1.87e-1 \pm 1.33e-1$	$2.75e-1 \pm 1.89e-1$	$8.88e+0 \pm 8.82e+0$
4	$5.53e-2 \pm 2.36e-2$	$1.83e-1 \pm 1.41e-1$	$4.20e+0 \pm 7.96e+0$	$4.31e+0 \pm 4.40e+0$
5	$8.55e-2 \pm 4.28e-2$	$1.00e-1 \pm 5.72e-2$	$7.05e-1 \pm 1.21e+0$	$1.78e+0 \pm 1.43e+0$

F.1.3. HOPPERPHYSICS

 Table 9. Effect of spline degree on MSE performance of SplineFlow on hopperphysics simulations across missingness probabilities p .

Degree	$p = 0$	$p = 0.25$	$p = 0.5$	$p = 0.75$
1	$1.41e+0 \pm 1.72e-1$	$1.43e+0 \pm 2.98e-2$	$1.83e+0 \pm 6.19e-2$	$3.34e+0 \pm 4.30e-1$
2	$6.60e+0 \pm 2.35e+0$	$5.39e+1 \pm 2.47e+1$	$2.80e+2 \pm 5.93e+1$	$1.00e+3 \pm 6.07e+1$
3	$1.25e+1 \pm 8.86e+0$	$3.91e+2 \pm 1.80e+2$	$6.38e+4 \pm 1.24e+4$	$1.73e+4 \pm 1.56e+3$
4	$1.63e+1 \pm 1.29e+1$	$1.41e+5 \pm 2.11e+4$	$4.64e+5 \pm 1.50e+5$	$1.20e+5 \pm 6.57e+4$
5	$2.26e+1 \pm 6.33e+0$	$8.95e+5 \pm 1.36e+5$	$6.71e+5 \pm 1.30e+5$	$9.25e+4 \pm 2.44e+4$

 F.2. SDE Dynamics (ablations with order k) for linear, non-linear and oscillatory systems

From the ablation study in this section, we observe that higher-degree B-splines are useful in the stochastic case for modeling nonlinear systems such as Lotka–Volterra.

 F.2.1. EXPONENTIAL DECAY ($p = 0$)

Table 10. Effect of spline order on Exp-Decay performance.

Degree	MSE_{PODE}	MSE_{SDE}	Wasserstein	MMD	Energy
1	$3.91e-1 \pm 4.23e-3$	$4.56e-1 \pm 8.27e-3$	$3.31e-1 \pm 2.83e-3$	$2.73e-2 \pm 2.48e-3$	$6.94e-2 \pm 1.08e-3$
2	$1.25e+0 \pm 4.04e-1$	$2.38e+0 \pm 5.77e-1$	$7.94e-1 \pm 1.78e-1$	$3.38e-2 \pm 3.08e-3$	$1.12e-1 \pm 1.67e-2$
3	$8.22e-1 \pm 6.78e-2$	$2.03e+0 \pm 4.47e-1$	$6.87e-1 \pm 1.70e-1$	$3.85e-2 \pm 1.01e-2$	$1.25e-1 \pm 3.65e-2$
4	$1.20e+0 \pm 6.28e-1$	$4.74e+0 \pm 4.43e+0$	$1.17e+0 \pm 8.69e-1$	$3.46e-2 \pm 1.40e-2$	$1.30e-1 \pm 7.66e-2$
5	$1.27e+0 \pm 3.89e-1$	$9.89e+0 \pm 1.17e+1$	$1.49e+0 \pm 1.31e+0$	$6.13e-2 \pm 1.22e-2$	$2.26e-1 \pm 9.57e-2$

 F.2.2. EXPONENTIAL DECAY ($p = 0.25$)

 Table 11. Effect of B-spline degree on Exp-decay performance for $p = 0.25$.

Degree	MSE_{PODE}	MSE_{SDE}	Wasserstein	MMD	Energy
1	$3.66e-1 \pm 6.08e-3$	$4.70e-1 \pm 5.90e-3$	$2.51e-1 \pm 5.53e-3$	$1.51e-2 \pm 1.03e-3$	$4.12e-2 \pm 3.14e-3$
2	$7.30e-1 \pm 1.41e-1$	$1.49e+0 \pm 3.84e-2$	$5.52e-1 \pm 3.67e-2$	$4.28e-2 \pm 1.87e-2$	$1.43e-1 \pm 6.38e-2$
3	$1.37e+0 \pm 8.59e-1$	$2.55e+0 \pm 9.96e-1$	$7.75e-1 \pm 2.18e-1$	$4.36e-2 \pm 1.19e-2$	$1.47e-1 \pm 4.29e-2$
4	$8.48e-1 \pm 2.68e-1$	$2.73e+0 \pm 1.64e+0$	$8.58e-1 \pm 3.85e-1$	$4.18e-2 \pm 7.33e-3$	$1.38e-1 \pm 3.88e-2$
5	$3.12e+0 \pm 1.10e+0$	$4.41e+0 \pm 8.47e-1$	$1.17e+0 \pm 1.97e-1$	$6.01e-2 \pm 1.21e-2$	$2.60e-1 \pm 4.65e-2$

F.2.3. EXPONENTIAL DECAY ($p = 0.5$)

 Table 12. Effect of B-spline degree on Exp-decay performance for $p = 0.5$.

Degree	MSE_{PODE}	MSE_{SDE}	Wasserstein	MMD	Energy
1	$3.76e-1 \pm 3.30e-3$	$5.30e-1 \pm 6.59e-3$	$1.95e-1 \pm 1.42e-3$	$7.42e-3 \pm 3.31e-4$	$2.40e-2 \pm 1.36e-3$
2	$6.44e-1 \pm 5.12e-2$	$1.80e+0 \pm 5.27e-1$	$5.92e-1 \pm 1.49e-1$	$2.92e-2 \pm 8.18e-3$	$8.90e-2 \pm 1.62e-2$
3	$6.52e-1 \pm 9.32e-2$	$1.61e+0 \pm 9.35e-2$	$5.57e-1 \pm 4.34e-2$	$2.34e-2 \pm 9.21e-3$	$7.47e-2 \pm 2.55e-2$
4	$8.61e-1 \pm 3.17e-1$	$2.78e+0 \pm 1.86e+0$	$8.49e-1 \pm 4.06e-1$	$3.21e-2 \pm 1.25e-2$	$1.34e-1 \pm 5.61e-2$
5	$2.75e+0 \pm 2.96e+0$	$3.53e+0 \pm 3.21e+0$	$9.04e-1 \pm 6.04e-1$	$7.77e-2 \pm 5.26e-2$	$3.93e-1 \pm 3.49e-1$

 F.2.4. EXPONENTIAL DECAY ($p = 0.75$)

 Table 13. Effect of B-spline degree on Exp-decay performance for $p = 0.75$.

Degree	MSE_{PODE}	MSE_{SDE}	Wasserstein	MMD	Energy
1	$4.19e-1 \pm 5.87e-3$	$6.77e-1 \pm 8.23e-3$	$1.42e-1 \pm 1.72e-2$	$2.06e-3 \pm 1.55e-3$	$1.51e-2 \pm 5.15e-3$
2	$7.83e-1 \pm 4.41e-2$	$2.24e+0 \pm 1.00e+0$	$7.53e-1 \pm 2.53e-1$	$3.91e-2 \pm 9.25e-3$	$1.43e-1 \pm 5.00e-2$
3	$9.82e-1 \pm 7.21e-2$	$5.56e+0 \pm 3.84e+0$	$1.39e+0 \pm 6.96e-1$	$4.30e-2 \pm 1.32e-2$	$1.69e-1 \pm 3.47e-2$
4	$1.12e+0 \pm 9.37e-1$	$2.61e+0 \pm 5.93e-1$	$9.23e-1 \pm 1.44e-1$	$5.42e-2 \pm 2.47e-2$	$2.26e-1 \pm 1.46e-1$
5	$3.18e+5 \pm 4.50e+5$	$3.03e+5 \pm 4.23e+5$	$1.99e+2 \pm 2.47e+2$	$2.38e-1 \pm 2.83e-1$	$2.61e+2 \pm 3.68e+2$

 F.2.5. LOTKA–VOLTERRA ($p = 0$)

Table 14. Effect of spline order on Lotka–Volterra performance.

Degree	MSE_{PODE}	MSE_{SDE}	Wasserstein	MMD	Energy
1	$4.70e-1 \pm 9.54e-2$	$4.69e-1 \pm 9.23e-2$	$4.27e-1 \pm 7.98e-2$	$1.12e-1 \pm 6.87e-2$	$4.26e-1 \pm 2.38e-1$
2	$2.68e-1 \pm 1.44e-2$	$2.73e-1 \pm 1.37e-2$	$2.94e-1 \pm 3.16e-3$	$4.21e-2 \pm 3.45e-3$	$1.56e-1 \pm 1.33e-2$
3	$3.03e-1 \pm 6.56e-3$	$3.03e-1 \pm 1.10e-2$	$3.21e-1 \pm 8.22e-3$	$4.64e-2 \pm 3.21e-3$	$1.74e-1 \pm 1.36e-2$
4	$3.47e-1 \pm 3.19e-2$	$3.47e-1 \pm 3.10e-2$	$3.60e-1 \pm 2.25e-2$	$6.97e-2 \pm 1.63e-2$	$2.60e-1 \pm 5.59e-2$
5	$3.28e-1 \pm 2.62e-2$	$3.30e-1 \pm 2.62e-2$	$3.50e-1 \pm 3.36e-2$	$6.87e-2 \pm 2.85e-2$	$2.52e-1 \pm 9.45e-2$

 F.2.6. LOTKA–VOLTERRA ($p = 0.25$)

 Table 15. Effect of B-spline degree on Lotka–Volterra performance for $p = 0.25$.

Degree	MSE_{PODE}	MSE_{SDE}	Wasserstein	MMD	Energy
1	$5.22e-1 \pm 1.72e-1$	$5.24e-1 \pm 1.71e-1$	$4.56e-1 \pm 1.33e-1$	$1.32e-1 \pm 1.11e-1$	$4.89e-1 \pm 3.77e-1$
2	$3.40e-1 \pm 5.04e-2$	$3.38e-1 \pm 4.76e-2$	$3.20e-1 \pm 1.01e-2$	$4.57e-2 \pm 2.87e-3$	$1.82e-1 \pm 1.18e-2$
3	$3.34e-1 \pm 5.05e-2$	$3.39e-1 \pm 4.86e-2$	$3.37e-1 \pm 1.39e-2$	$6.22e-2 \pm 1.12e-2$	$2.47e-1 \pm 5.83e-2$
4	$3.18e-1 \pm 3.58e-2$	$3.21e-1 \pm 3.21e-2$	$3.19e-1 \pm 1.21e-2$	$4.45e-2 \pm 5.03e-3$	$1.75e-1 \pm 2.60e-2$
5	$2.81e-1 \pm 1.70e-2$	$2.83e-1 \pm 1.54e-2$	$3.19e-1 \pm 5.33e-3$	$4.83e-2 \pm 3.97e-3$	$1.83e-1 \pm 1.57e-2$

F.2.7. LOTKA–VOLTERRA ($p = 0.5$)

 Table 16. Effect of B-spline degree on Lotka–Volterra performance for $p = 0.5$.

Degree	MSE_{PODE}	MSE_{SDE}	Wasserstein	MMD	Energy
1	$3.82e-1 \pm 6.10e-2$	$3.83e-1 \pm 5.94e-2$	$3.70e-1 \pm 1.68e-2$	$7.09e-2 \pm 4.52e-3$	$2.75e-1 \pm 1.38e-2$
2	$4.11e-1 \pm 4.68e-2$	$4.15e-1 \pm 4.79e-2$	$3.74e-1 \pm 3.81e-2$	$6.24e-2 \pm 9.27e-3$	$2.59e-1 \pm 3.66e-2$
3	$2.88e-1 \pm 2.32e-2$	$2.85e-1 \pm 2.54e-2$	$3.10e-1 \pm 1.16e-2$	$4.42e-2 \pm 3.80e-3$	$1.64e-1 \pm 2.32e-2$
4	$3.70e-1 \pm 1.10e-1$	$3.72e-1 \pm 1.11e-1$	$3.48e-1 \pm 4.99e-2$	$5.39e-2 \pm 2.09e-2$	$2.22e-1 \pm 1.02e-1$
5	$3.19e-1 \pm 2.96e-2$	$3.23e-1 \pm 3.05e-2$	$3.11e-1 \pm 1.57e-2$	$4.50e-2 \pm 2.94e-3$	$1.79e-1 \pm 7.45e-3$

 F.2.8. LOTKA–VOLTERRA ($p = 0.75$)

 Table 17. Effect of B-spline degree on Lotka–Volterra performance for $p = 0.75$.

Degree	MSE_{PODE}	MSE_{SDE}	Wasserstein	MMD	Energy
1	$4.98e-1 \pm 1.36e-1$	$4.99e-1 \pm 1.35e-1$	$4.53e-1 \pm 4.31e-2$	$1.21e-1 \pm 1.03e-2$	$4.53e-1 \pm 7.16e-2$
2	$4.30e-1 \pm 7.67e-2$	$4.33e-1 \pm 7.35e-2$	$3.97e-1 \pm 6.21e-2$	$8.44e-2 \pm 3.38e-2$	$3.30e-1 \pm 1.15e-1$
3	$3.77e-1 \pm 5.73e-2$	$3.78e-1 \pm 5.48e-2$	$3.61e-1 \pm 4.04e-2$	$5.57e-2 \pm 9.43e-3$	$2.23e-1 \pm 4.77e-2$
4	$4.49e-1 \pm 1.40e-1$	$4.43e-1 \pm 1.29e-1$	$3.55e-1 \pm 4.84e-2$	$6.56e-2 \pm 1.72e-2$	$2.75e-1 \pm 9.15e-2$
5	$6.03e-1 \pm 2.33e-1$	$5.98e-1 \pm 2.31e-1$	$4.60e-1 \pm 7.29e-2$	$1.26e-1 \pm 4.30e-2$	$5.06e-1 \pm 1.91e-1$

 F.2.9. DAMPED HARMONIC OSCILLATOR ($p = 0$)

Table 18. Effect of spline order on damped harmonic oscillator performance.

Degree	MSE_{PODE}	MSE_{SDE}	Wasserstein	MMD	Energy
1	$8.95e-1 \pm 5.12e-3$	$9.70e-1 \pm 9.41e-3$	$4.10e-1 \pm 4.41e-3$	$4.19e-2 \pm 1.54e-3$	$1.12e-1 \pm 7.12e-3$
2	$1.78e+0 \pm 1.96e-1$	$8.02e+0 \pm 4.45e+0$	$1.58e+0 \pm 6.03e-1$	$7.48e-3 \pm 1.30e-3$	$8.23e-2 \pm 3.24e-2$
3	$5.51e+0 \pm 2.89e+0$	$1.30e+1 \pm 7.52e+0$	$2.07e+0 \pm 6.98e-1$	$2.08e-2 \pm 1.41e-2$	$2.06e-1 \pm 1.72e-1$
4	$9.23e+0 \pm 2.11e+0$	$1.56e+1 \pm 2.84e+0$	$2.43e+0 \pm 2.60e-1$	$1.69e-2 \pm 7.13e-3$	$1.90e-1 \pm 4.45e-2$
5	$8.53e+0 \pm 5.52e+0$	$2.21e+1 \pm 1.21e+1$	$3.04e+0 \pm 7.89e-1$	$2.13e-2 \pm 1.77e-3$	$2.67e-1 \pm 1.09e-1$

 F.2.10. DAMPED HARMONIC OSCILLATOR ($p = 0.25$)

 Table 19. Effect of B-spline degree on Damped-Harmonic performance for $p = 0.25$.

Degree	MSE_{PODE}	MSE_{SDE}	Wasserstein	MMD	Energy
1	$7.99e-1 \pm 1.57e-2$	$9.14e-1 \pm 2.28e-2$	$3.65e-1 \pm 2.11e-2$	$3.42e-2 \pm 4.34e-3$	$9.17e-2 \pm 1.07e-2$
2	$2.22e+0 \pm 8.18e-1$	$3.48e+0 \pm 7.77e-1$	$8.66e-1 \pm 1.83e-1$	$1.43e-2 \pm 2.24e-3$	$9.77e-2 \pm 7.13e-3$
3	$1.49e+0 \pm 3.66e-2$	$6.24e+0 \pm 2.46e+0$	$1.33e+0 \pm 4.36e-1$	$7.18e-3 \pm 3.63e-3$	$7.58e-2 \pm 2.36e-2$
4	$4.11e+0 \pm 8.82e-1$	$9.91e+0 \pm 3.36e+0$	$1.76e+0 \pm 2.72e-1$	$2.62e-2 \pm 2.77e-3$	$1.96e-1 \pm 2.59e-2$
5	$7.85e+0 \pm 3.86e+0$	$1.52e+1 \pm 7.33e+0$	$2.34e+0 \pm 7.83e-1$	$3.32e-2 \pm 2.33e-2$	$3.66e-1 \pm 1.77e-1$

F.2.11. DAMPED HARMONIC OSCILLATOR ($p = 0.5$)

 Table 20. Effect of B-spline degree on Damped-Harmonic performance for $p = 0.5$.

Degree	MSE_{PODE}	MSE_{SDE}	Wasserstein	MMD	Energy
1	$8.05e-1 \pm 8.73e-3$	$9.81e-1 \pm 3.99e-2$	$3.21e-1 \pm 2.84e-2$	$2.18e-2 \pm 5.59e-3$	$6.87e-2 \pm 1.21e-2$
2	$1.61e+0 \pm 4.11e-1$	$9.25e+0 \pm 7.31e+0$	$1.52e+0 \pm 9.81e-1$	$1.23e-2 \pm 7.06e-3$	$1.04e-1 \pm 6.55e-2$
3	$1.34e+0 \pm 2.35e-1$	$3.23e+0 \pm 1.62e+0$	$7.52e-1 \pm 3.50e-1$	$1.05e-2 \pm 4.37e-3$	$7.49e-2 \pm 2.28e-2$
4	$1.64e+0 \pm 4.51e-1$	$1.38e+1 \pm 1.04e+1$	$2.08e+0 \pm 1.07e+0$	$1.02e-2 \pm 3.90e-3$	$9.98e-2 \pm 4.27e-2$
5	$4.26e+0 \pm 2.48e+0$	$2.05e+1 \pm 2.01e+1$	$2.71e+0 \pm 1.93e+0$	$5.87e-3 \pm 2.05e-3$	$6.62e-2 \pm 2.93e-2$

 F.2.12. DAMPED HARMONIC OSCILLATOR ($p = 0.75$)

 Table 21. Effect of B-spline degree on Damped-Harmonic performance for $p = 0.75$.

Degree	MSE_{PODE}	MSE_{SDE}	Wasserstein	MMD	Energy
1	$9.38e-1 \pm 2.89e-2$	$1.17e+0 \pm 1.17e-2$	$2.86e-1 \pm 1.10e-2$	$1.24e-2 \pm 7.65e-4$	$5.28e-2 \pm 4.89e-3$
2	$2.24e+0 \pm 6.32e-1$	$7.16e+0 \pm 5.03e-1$	$1.56e+0 \pm 1.18e-1$	$1.29e-2 \pm 4.25e-3$	$1.02e-1 \pm 3.60e-2$
3	$3.34e+0 \pm 2.64e+0$	$8.62e+0 \pm 5.79e+0$	$1.43e+0 \pm 5.99e-1$	$1.13e-2 \pm 1.98e-3$	$9.04e-2 \pm 1.63e-2$
4	$7.48e+0 \pm 8.12e+0$	$3.67e+1 \pm 2.28e+1$	$3.83e+0 \pm 1.39e+0$	$3.72e-2 \pm 3.14e-2$	$2.98e-1 \pm 2.59e-1$
5	$8.79e+1 \pm 1.22e+2$	$4.87e+1 \pm 5.88e+1$	$3.11e+0 \pm 2.19e+0$	$3.30e-2 \pm 3.02e-2$	$3.06e-1 \pm 3.25e-1$

F.3. Chaotic Dynamics

In this section, we conduct ablation studies on the Lorenz system, which is highly chaotic. We observe that higher-degree interpolants are especially effective for modeling stochastic chaotic dynamics, whereas all degree $m > 2$ variants perform better than the linear baseline in the deterministic cases.

 F.3.1. LORENZ ODE ($p = 0$)

 Table 22. Lorenz system results for regularly sampled observations $p = 0$.

Degree	MSE
1	$1.380 \pm 1.890e-02$
2	$6.800e-01 \pm 1.520e-02$
3	$6.400e-01 \pm 3.790e-03$
4	$7.800e-01 \pm 1.320e-01$
5	$9.200e-01 \pm 7.360e-02$

 F.3.2. LORENZ SDE ($p = 0$)

Table 23. Effect of spline order on stochastic Lorenz system performance.

Degree	MSE_{PODE}	MSE_{SDE}	Wasserstein	MMD	Energy
1	$2.21e+0 \pm 9.71e-3$	$2.21e+0 \pm 9.67e-3$	$6.31e-1 \pm 2.03e-3$	$1.30e-1 \pm 1.22e-3$	$4.01e-1 \pm 3.50e-3$
2	$2.19e+0 \pm 1.38e-2$	$2.19e+0 \pm 1.88e-2$	$6.30e-1 \pm 1.90e-3$	$1.29e-1 \pm 2.21e-4$	$3.98e-1 \pm 1.52e-3$
3	$4.82e+0 \pm 4.96e+0$	$3.71e+0 \pm 3.37e+0$	$9.31e-1 \pm 9.85e-1$	$7.44e-3 \pm 6.53e-3$	$5.61e-2 \pm 3.44e-2$
4	$1.23e+0 \pm 4.01e-2$	$1.23e+0 \pm 5.62e-2$	$1.80e-1 \pm 1.47e-2$	$4.51e-3 \pm 1.79e-3$	$3.66e-2 \pm 7.65e-3$
5	$1.36e+0 \pm 6.41e-2$	$1.50e+0 \pm 2.46e-1$	$3.07e-1 \pm 1.49e-1$	$6.44e-3 \pm 1.73e-3$	$4.47e-2 \pm 1.08e-2$

F.4. Cellular Dynamics

F.4.1. BRAIN REGENERATION DATA

From the ablation study, we observe that higher-degree variants are especially better-performing when working with PHATE embeddings. While the degree $m = 2$ is often the optimal variant for PCA embedding. This aligns with PHATE embeddings, which are meant to capture structural organization within datasets and thus benefit from B-splines.

F.4.2. PHATE EMBEDDING: INTERPOLATION

Table 24. Effect of B-spline degree on PHATE interpolation performance.

Degree	Wasserstein	MMD	Energy
1	$7.714e-01 \pm 1.250e-02$	$4.813e-01 \pm 1.740e-02$	$1.391e+00 \pm 7.250e-02$
2	$6.421e-01 \pm 5.280e-02$	$3.088e-01 \pm 2.570e-02$	$9.172e-01 \pm 9.580e-02$
3	$6.519e-01 \pm 2.100e-02$	$3.174e-01 \pm 5.200e-03$	$9.277e-01 \pm 2.030e-02$
4	$6.548e-01 \pm 2.930e-02$	$3.120e-01 \pm 2.020e-02$	$9.189e-01 \pm 7.080e-02$
5	$6.066e-01 \pm 2.710e-02$	$2.846e-01 \pm 6.600e-03$	$8.152e-01 \pm 2.140e-02$

F.4.3. PHATE EMBEDDING: EXTRAPOLATION

Table 25. Effect of B-spline degree on PHATE extrapolation performance.

Degree	Wasserstein	MMD	Energy
1	$1.588 \pm 2.270e-02$	$9.796e-01 \pm 4.000e-03$	$3.843 \pm 3.700e-02$
2	$1.584 \pm 3.670e-02$	$9.654e-01 \pm 6.300e-03$	$3.787 \pm 6.170e-02$
3	$1.536 \pm 1.700e-02$	$9.623e-01 \pm 2.700e-03$	$3.761 \pm 2.500e-02$
4	$1.587 \pm 1.920e-02$	$9.550e-01 \pm 8.700e-03$	$3.740 \pm 4.240e-02$
5	$1.545 \pm 2.720e-02$	$9.644e-01 \pm 3.200e-03$	$3.751 \pm 1.290e-02$

F.4.4. PCA EMBEDDING: INTERPOLATION

Table 26. Effect of B-spline degree on PCA interpolation performance.

Degree	Wasserstein	MMD	Energy
1	$8.719e-01 \pm 3.180e-02$	$6.320e-02 \pm 3.600e-03$	$1.120 \pm 4.510e-02$
2	$8.380e-01 \pm 1.370e-02$	$5.820e-02 \pm 2.500e-03$	$1.019 \pm 3.930e-02$
3	$8.346e-01 \pm 1.670e-02$	$6.030e-02 \pm 1.200e-03$	$1.035 \pm 1.660e-02$
4	$8.502e-01 \pm 1.110e-02$	$6.140e-02 \pm 3.000e-03$	$1.063 \pm 3.660e-02$
5	$8.512e-01 \pm 1.940e-02$	$6.150e-02 \pm 2.600e-03$	$1.063 \pm 3.940e-02$

F.4.5. PCA EMBEDDING: EXTRAPOLATION

Table 27. Effect of B-spline degree on PCA extrapolation performance.

Degree	Wasserstein	MMD	Energy
1	$8.434e-01 \pm 2.500e-02$	$1.730e-01 \pm 8.800e-03$	$1.869 \pm 2.100e-02$
2	$8.040e-01 \pm 3.720e-02$	$1.292e-01 \pm 6.800e-03$	$1.645 \pm 5.660e-02$
3	$8.622e-01 \pm 4.030e-02$	$1.415e-01 \pm 7.900e-03$	$1.738 \pm 7.230e-02$
4	$8.206e-01 \pm 4.100e-02$	$1.355e-01 \pm 1.180e-02$	$1.736 \pm 8.500e-02$
5	$8.234e-01 \pm 1.070e-02$	$1.336e-01 \pm 1.310e-02$	$1.690 \pm 1.068e-01$

F.4.6. EMBRYOID DEVELOPMENT DATA

From the ablation study, we observe that, in almost all cases, the better-performing variant degree is greater than linear for both PHATE and PCA embeddings. The higher-degree variants are especially suitable for extrapolation settings with PCA embeddings.

F.4.7. PHATE EMBEDDING: INTERPOLATION

Table 28. Effect of B-spline degree on PHATE interpolation performance.

Degree	Wasserstein	MMD	Energy
1	2.355e-01 \pm 3.280e-02	2.783e-02 \pm 5.360e-03	7.954e-02 \pm 1.660e-02
2	2.745e-01 \pm 3.700e-02	1.768e-02 \pm 3.220e-03	6.331e-02 \pm 1.540e-02
3	2.071e-01 \pm 1.690e-02	1.260e-02 \pm 5.870e-04	3.963e-02 \pm 1.400e-03
4	2.560e-01 \pm 6.300e-02	1.592e-02 \pm 4.450e-03	5.462e-02 \pm 1.620e-02
5	2.217e-01 \pm 3.530e-02	1.408e-02 \pm 3.100e-03	4.467e-02 \pm 9.410e-03

F.4.8. PHATE EMBEDDING: EXTRAPOLATION

Table 29. Effect of B-spline degree on PHATE extrapolation performance.

Degree	Wasserstein	MMD	Energy
1	5.765e-01 \pm 5.860e-02	7.572e-02 \pm 1.110e-02	2.833e-01 \pm 4.370e-02
2	4.483e-01 \pm 4.410e-02	6.902e-02 \pm 1.700e-03	2.073e-01 \pm 2.960e-02
3	4.774e-01 \pm 6.720e-02	6.540e-02 \pm 9.270e-03	2.367e-01 \pm 5.200e-02
4	5.502e-01 \pm 7.380e-02	7.318e-02 \pm 1.650e-02	2.916e-01 \pm 8.900e-02
5	4.733e-01 \pm 6.450e-02	7.417e-02 \pm 3.690e-03	2.423e-01 \pm 2.410e-02

F.4.9. PCA EMBEDDING: INTERPOLATION

Table 30. Effect of B-spline degree on PCA interpolation performance.

Degree	Wasserstein	MMD	Energy
1	3.008e-01 \pm 6.130e-03	1.341e-02 \pm 7.060e-04	1.913e-01 \pm 8.150e-03
2	3.073e-01 \pm 1.260e-02	1.231e-02 \pm 5.310e-04	2.070e-01 \pm 9.860e-03
3	3.080e-01 \pm 1.510e-02	1.328e-02 \pm 1.680e-03	2.134e-01 \pm 2.560e-02
4	2.959e-01 \pm 1.460e-02	1.267e-02 \pm 3.110e-04	1.994e-01 \pm 9.340e-03
5	3.248e-01 \pm 9.690e-03	1.358e-02 \pm 4.650e-04	2.230e-01 \pm 1.100e-02

F.4.10. PCA EMBEDDING: EXTRAPOLATION

Table 31. Effect of B-spline degree on PCA extrapolation performance.

Degree	Wasserstein	MMD	Energy
1	5.652e-01 \pm 2.770e-02	3.352e-02 \pm 1.930e-03	6.546e-01 \pm 5.310e-02
2	5.861e-01 \pm 2.590e-02	3.790e-02 \pm 2.500e-03	7.244e-01 \pm 5.470e-02
3	5.387e-01 \pm 3.350e-02	3.583e-02 \pm 4.420e-03	6.895e-01 \pm 1.010e-01
4	5.389e-01 \pm 2.420e-02	3.469e-02 \pm 2.410e-03	6.588e-01 \pm 5.070e-02
5	5.871e-01 \pm 1.240e-02	3.842e-02 \pm 3.320e-03	7.504e-01 \pm 5.620e-02

G. Visualizations of Predicted Dynamics

In this section, we visualize the predicted trajectories alongside the ground truth in different spaces to further examine the learning performance of different methods (apart from quantitative metric performance). For irregularly sampled settings,

we choose $p = 0.75$ to reflect the most challenging scenarios. The trajectories predicted by our SplineFlow method can recover the ground-truth dynamics well, particularly outperforming other methods for the chaotic Lorenz system.

G.1. ODE Dynamics

G.1.1. HARMONIC OSCILLATOR ($p = 0.75$)

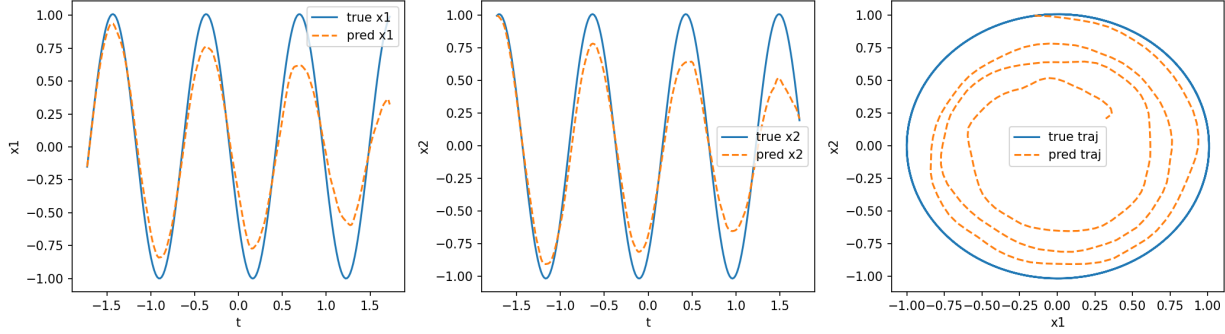


Figure 5. TFM evaluated path for Harmonic Oscillator.

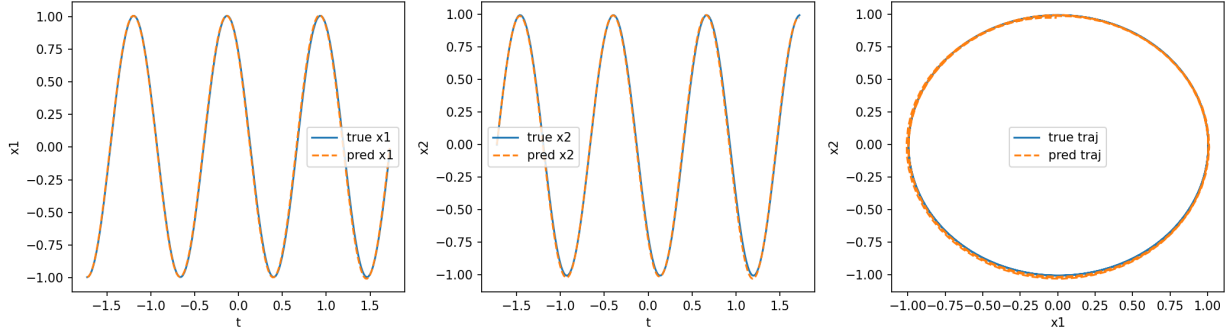


Figure 6. SplineFlow evaluated path for Harmonic Oscillator.

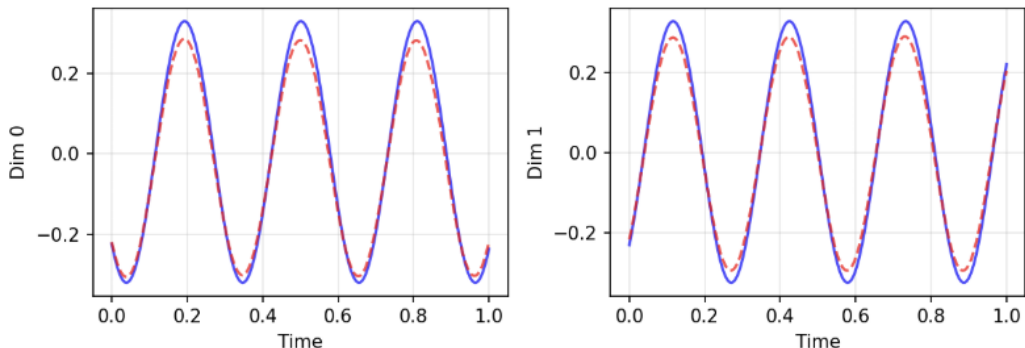


Figure 7. LatentODE evaluated path for Harmonic Oscillator.

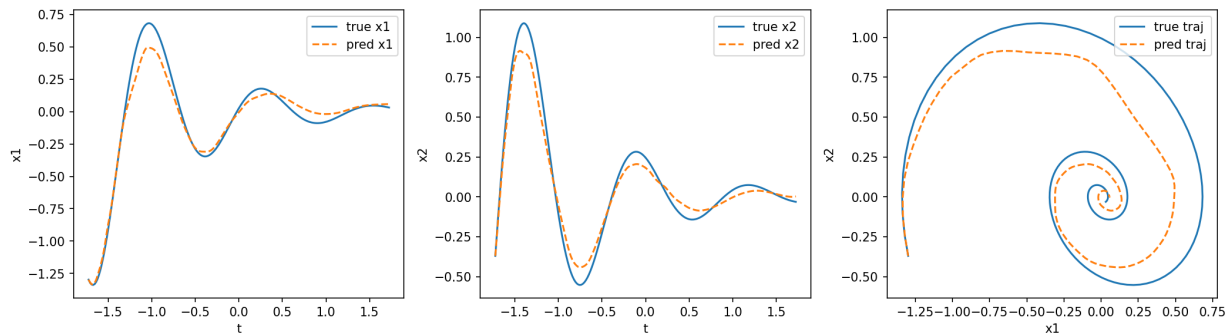
G.1.2. DAMPED HARMONIC OSCILLATOR ($p = 0.75$)


Figure 8. TFM evaluated path for Damped Harmonic Oscillator.

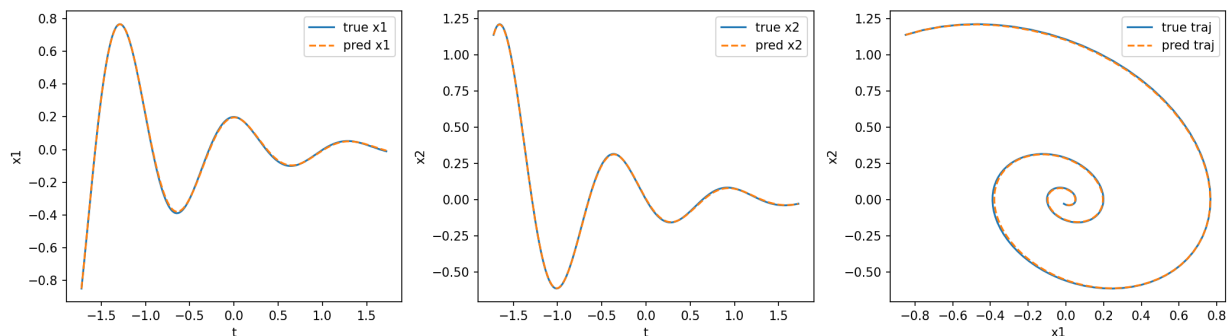


Figure 9. SplineFlow evaluated path for Damped Harmonic Oscillator.

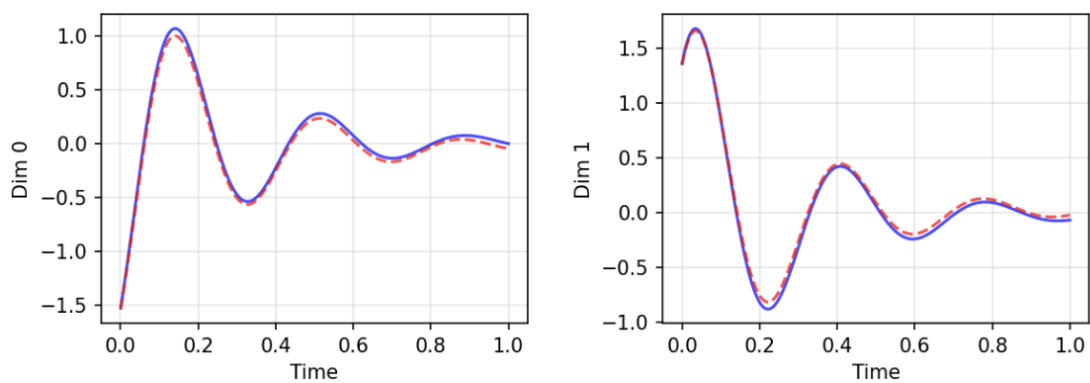


Figure 10. LatentODE evaluated path for Damped Harmonic Oscillator.

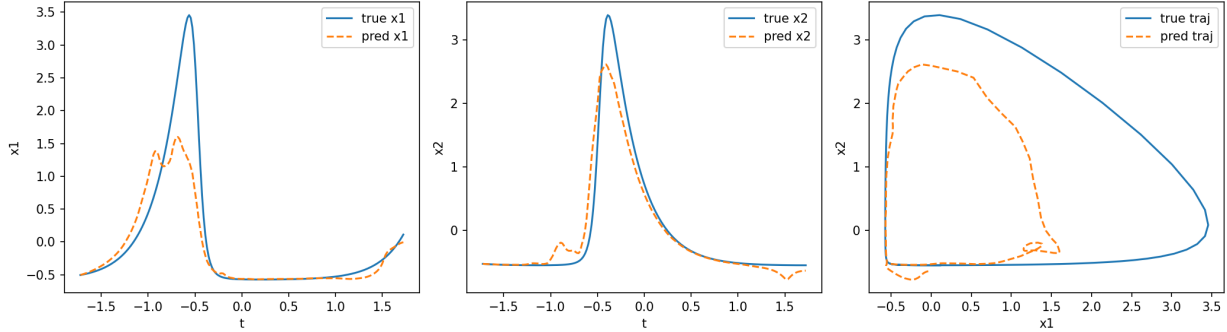
G.1.3. LOTKA–VOLTERRA ($p = 0.75$)


Figure 11. TFM evaluated path for Lotka–Volterra System.

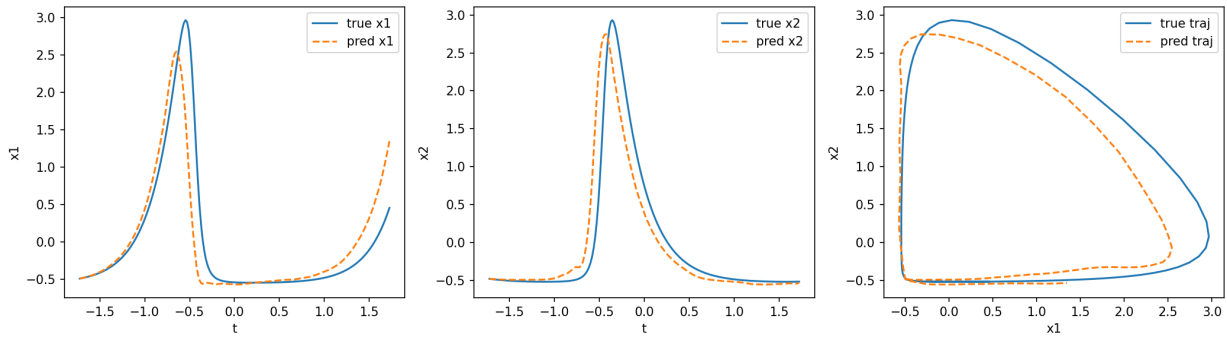


Figure 12. SplineFlow evaluated path for Lotka–Volterra System.

G.2. Chaotic Systems (Lorenz)

G.2.1. ADJOINT-METHODS ODE DYNAMICS

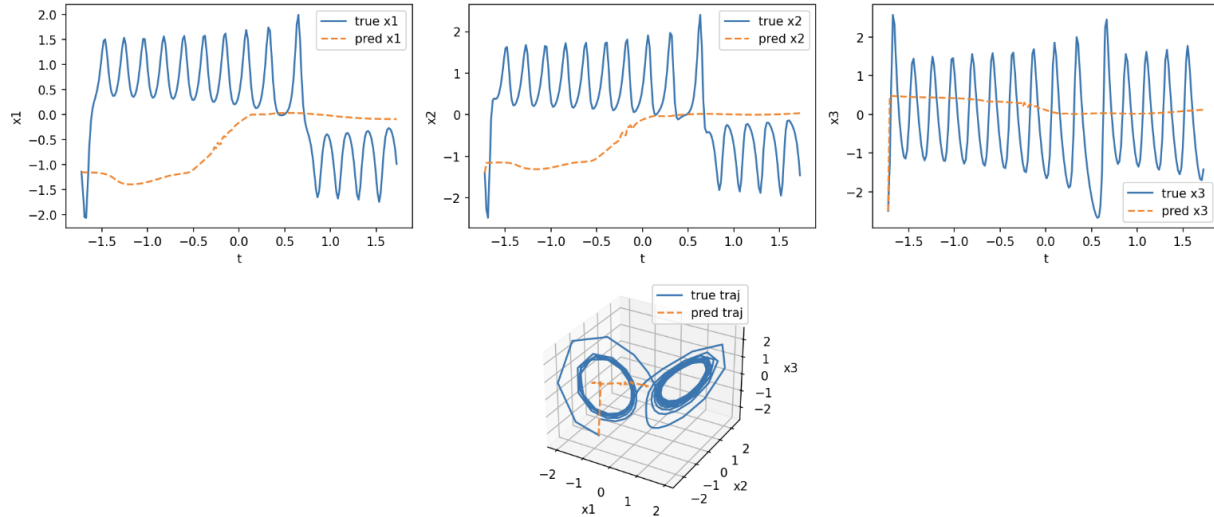


Figure 13. NeuralODE evaluated path for Lorenz System.

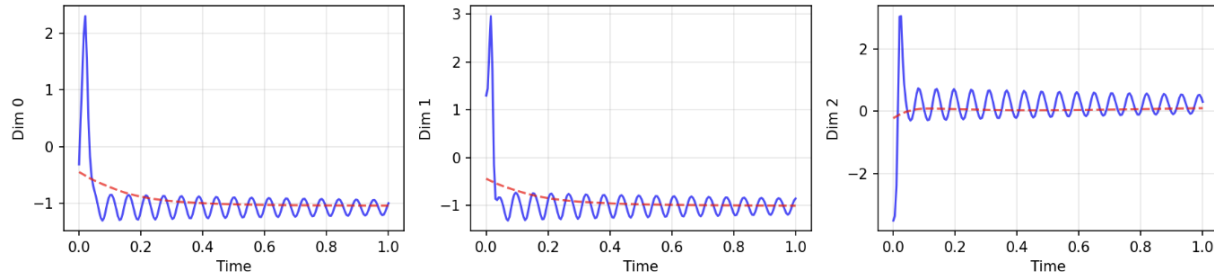


Figure 14. LatentODE evaluated path for Lorenz System.

G.2.2. TRAJECTORY FLOW MATCHING ODE DYNAMICS

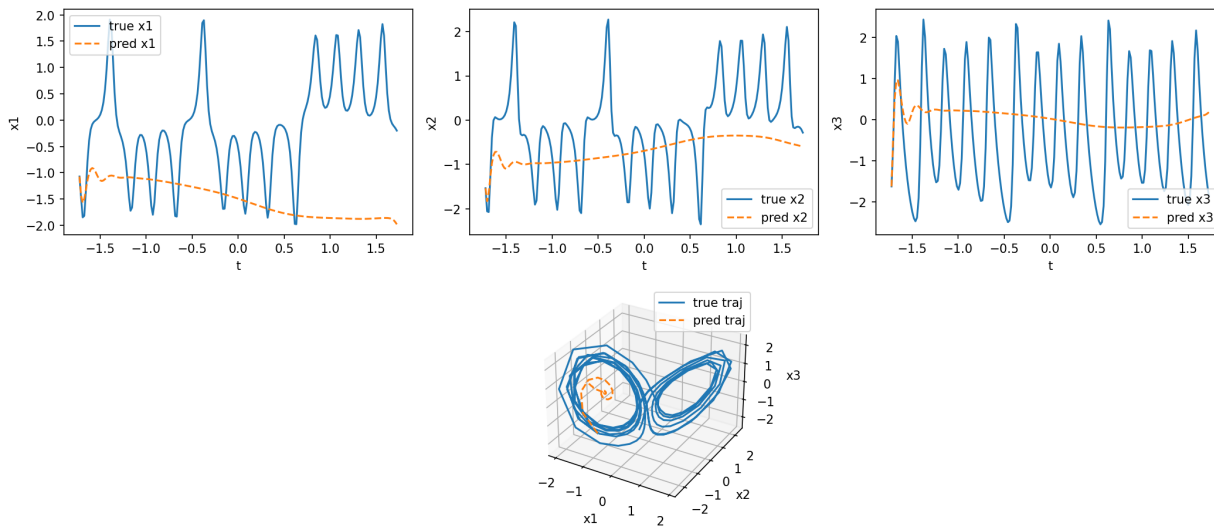


Figure 15. TFM evaluated path for Lorenz System.

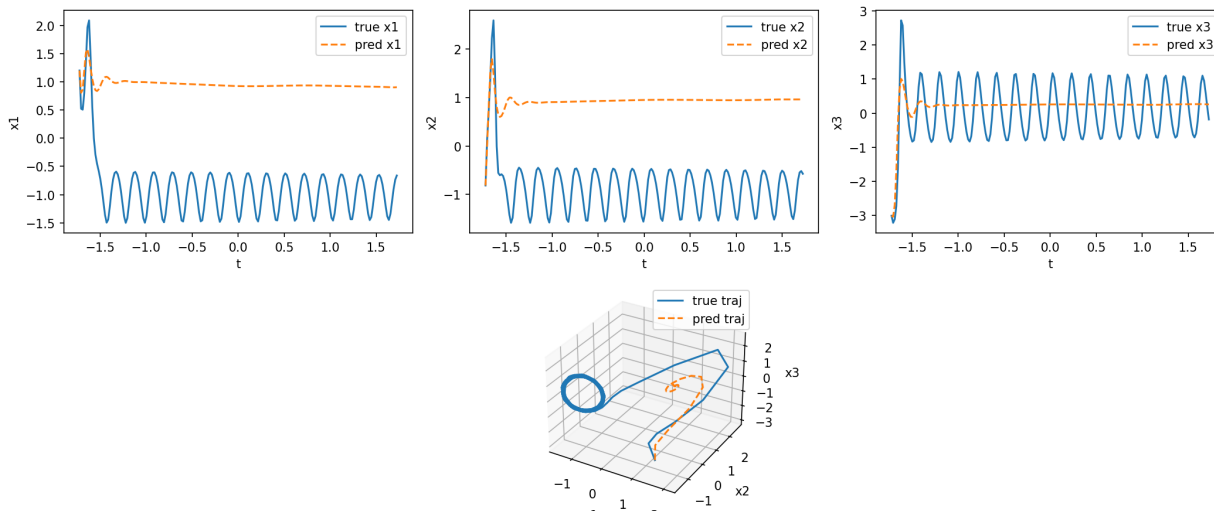


Figure 16. TFM evaluated path for Lorenz System.

G.2.3. SPLINEFLOW ODE DYNAMICS

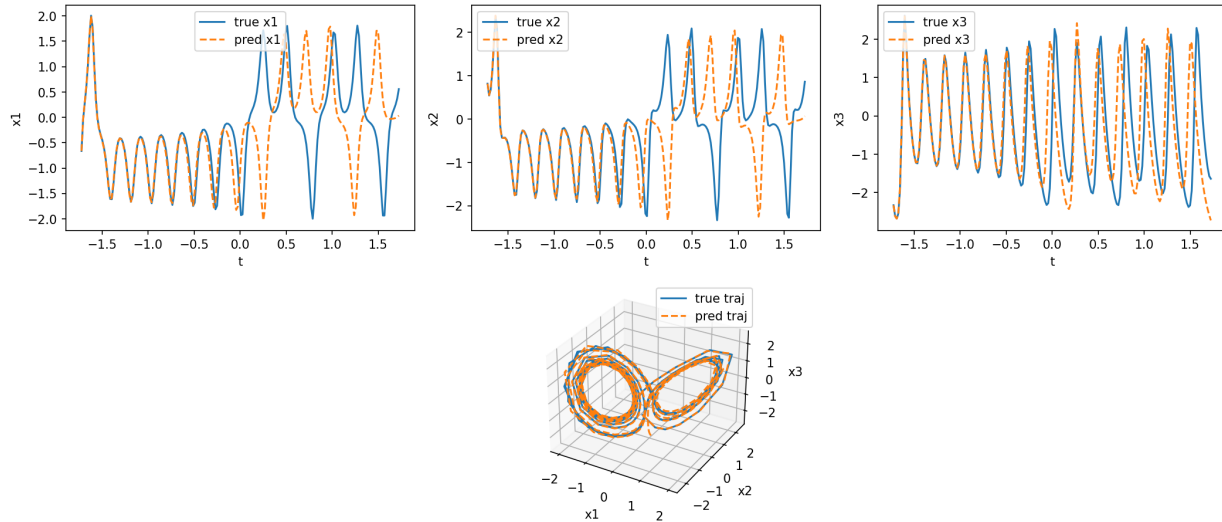


Figure 17. SplineFlow evaluated path for Lorenz System.

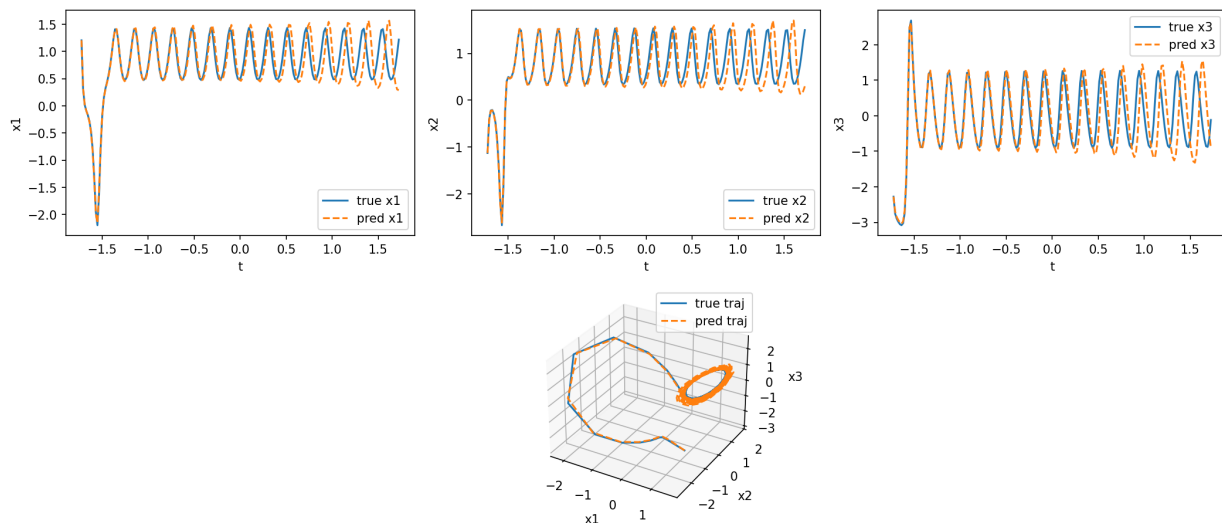


Figure 18. SplineFlow evaluated path for Lorenz System.

G.2.4. SF2M SDE DYNAMICS

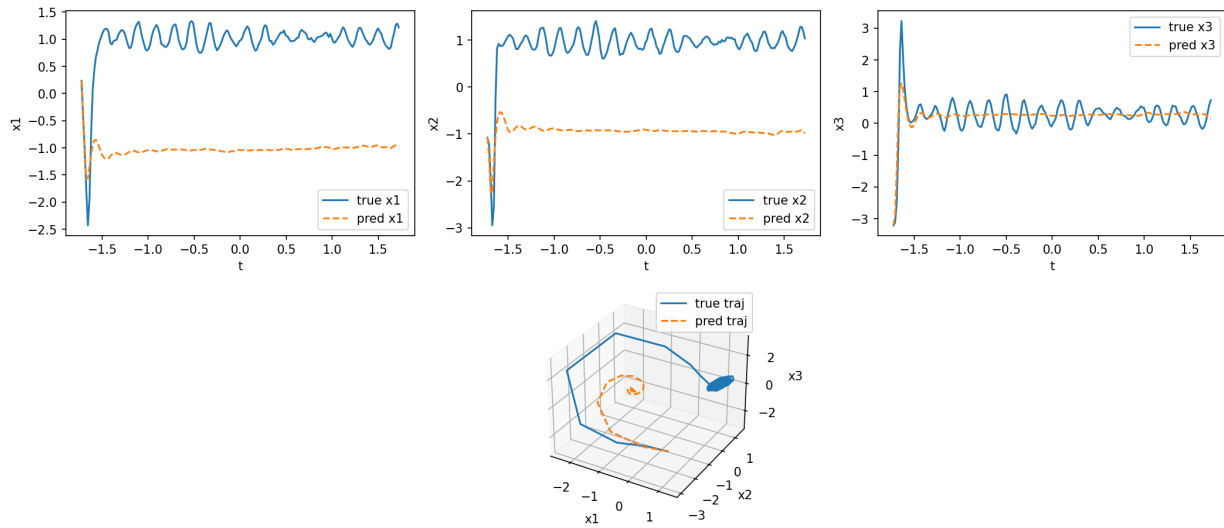


Figure 19. SF2M evaluated path for Lorenz System.

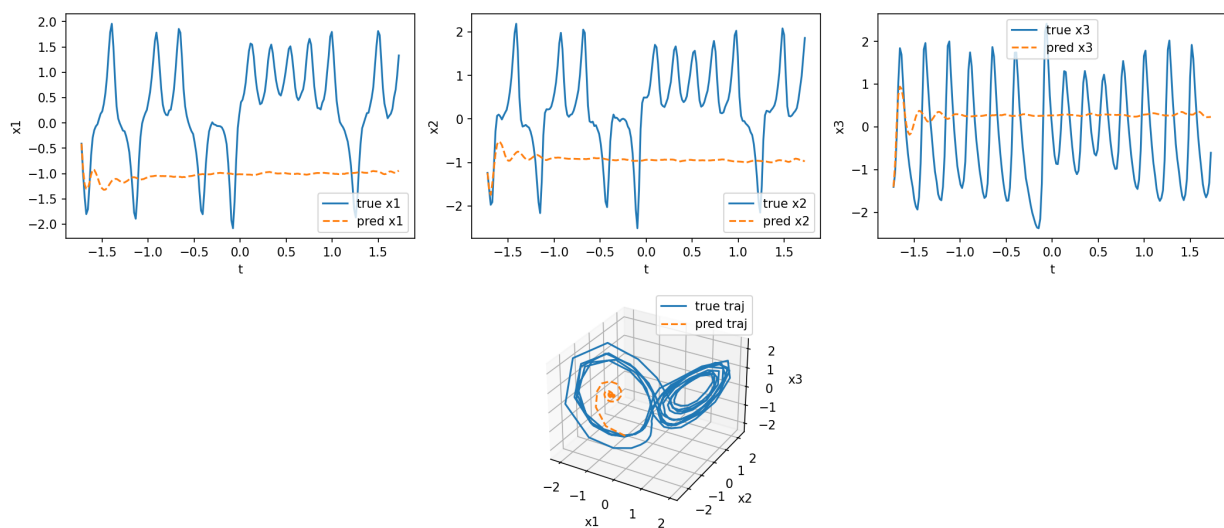


Figure 20. SF2M evaluated path for Lorenz System.

G.2.5. SPLINEFLOW SDE DYNAMICS

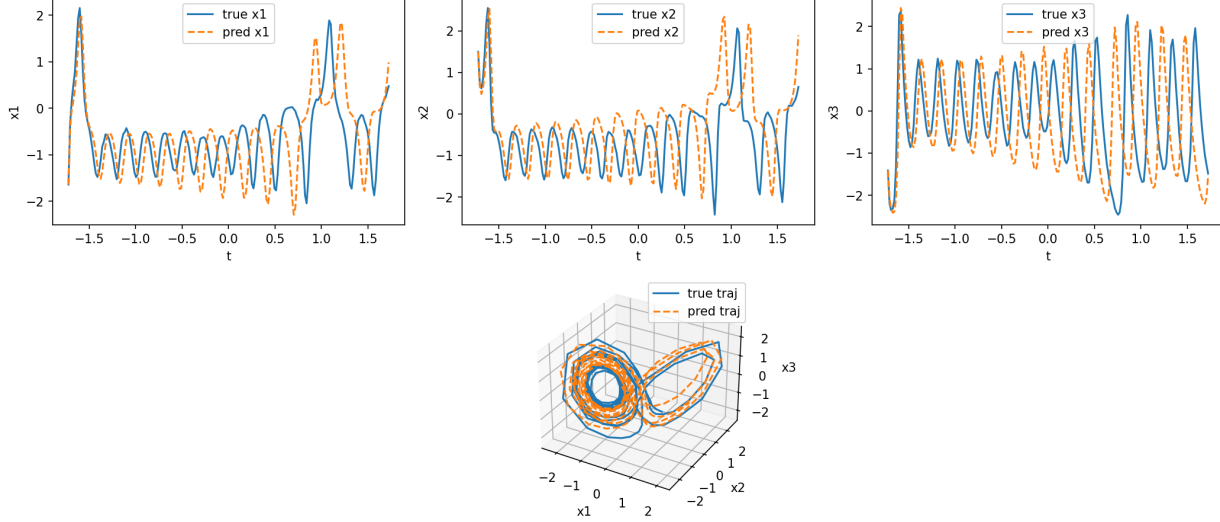


Figure 21. SplineFlow evaluated path for Lorenz System.

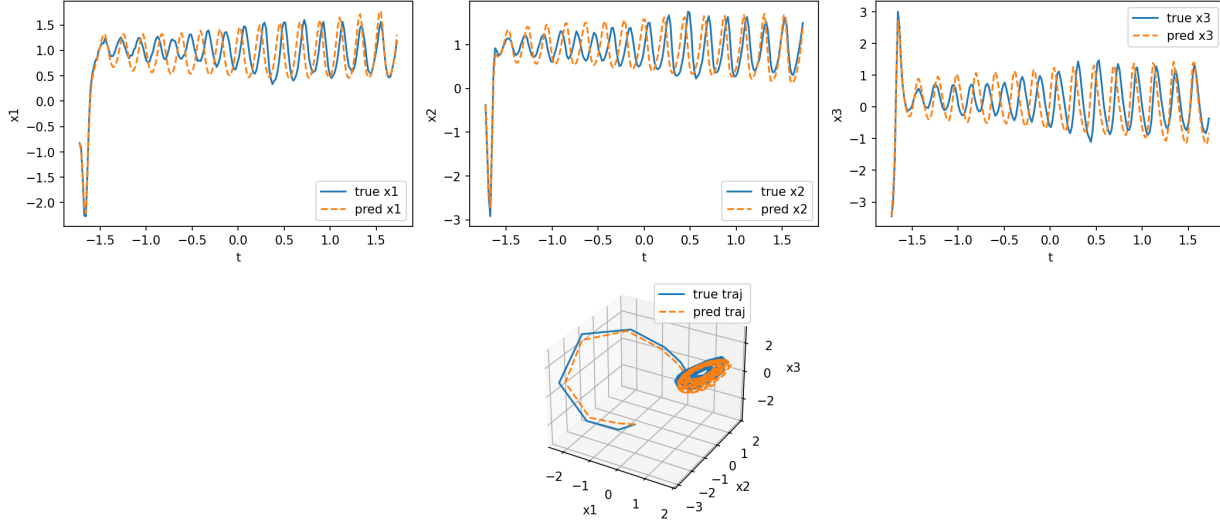


Figure 22. SplineFlow evaluated path for Lorenz System.

H. Expanded Experimental Results

 Table 32. Performance across SDE dynamics datasets for different metrics under regular sampling $p = 0$.

Dataset	Model	MSE (P-ODE)	MSE (SDE)	Wasserstein	MMD	Energy
Exp-decay	SF2M	3.911e-01 \pm 2.26e-03	4.770e-01 \pm 9.90e-03	3.053e-01 \pm 4.85e-03	2.400e-02 \pm 1.00e-03	6.100e-02 \pm 2.62e-03
	SplineFlow	3.906e-01 \pm 4.23e-03	4.557e-01 \pm 8.27e-03	3.305e-01 \pm 2.83e-03	2.700e-02 \pm 2.48e-03	6.941e-02 \pm 1.08e-03
Damped-Harmonic	SF2M	8.442e-01 \pm 1.54e-02	9.665e-01 \pm 3.29e-02	4.298e-01 \pm 7.40e-03	4.843e-02 \pm 2.96e-03	1.257e-01 \pm 3.74e-03
	SplineFlow	8.945e-01 \pm 5.12e-03	9.696e-01 \pm 9.41e-03	4.101e-01 \pm 4.41e-03	4.190e-02 \pm 1.54e-03	1.123e-01 \pm 7.12e-03
Lotka-Volterra	SF2M	4.583e-01 \pm 9.74e-02	4.607e-01 \pm 9.67e-02	4.435e-01 \pm 4.99e-02	1.255e-01 \pm 2.35e-02	4.653e-01 \pm 9.44e-02
	SplineFlow	2.685e-01 \pm 1.44e-02	2.730e-01 \pm 1.37e-02	2.939e-01 \pm 3.16e-03	4.213e-02 \pm 3.45e-03	1.560e-01 \pm 1.33e-02
Lorenz	SF2M	2.170e+00 \pm 7.94e-03	2.159e+00 \pm 8.35e-03	6.324e-01 \pm 7.61e-03	1.298e-01 \pm 2.56e-03	4.045e-01 \pm 1.08e-02
	SplineFlow	1.232e+00 \pm 4.01e-02	1.227e+00 \pm 5.62e-02	1.799e-01 \pm 1.47e-02	5.000e-03 \pm 1.79e-03	3.660e-02 \pm 7.65e-03

Table 33. Performance across SDE dynamics datasets for different metrics under irregular sampling $p > 0$.

Dataset	p	Model	MSE (P-ODE)	MSE (SDE)	Wasserstein	MMD	Energy
Exp-decay	0.25	SF2M	3.649e-01 ± 1.27e-03	4.659e-01 ± 6.30e-03	2.454e-01 ± 7.37e-03	1.469e-02 ± 1.15e-03	4.011e-02 ± 2.76e-03
		SplineFlow	3.660e-01 ± 6.08e-03	4.698e-01 ± 5.90e-03	2.508e-01 ± 5.53e-03	1.511e-02 ± 1.03e-03	4.121e-02 ± 3.14e-03
	0.5	SF2M	3.770e-01 ± 5.88e-03	5.235e-01 ± 1.07e-02	2.041e-01 ± 1.16e-02	9.091e-03 ± 1.93e-03	2.831e-02 ± 4.68e-03
		SplineFlow	3.763e-01 ± 3.30e-03	5.300e-01 ± 6.59e-03	1.946e-01 ± 1.42e-03	7.420e-03 ± 3.31e-04	2.399e-02 ± 1.36e-03
	0.75	SF2M	4.051e-01 ± 6.73e-03	6.468e-01 ± 1.07e-02	1.369e-01 ± 1.20e-02	1.477e-03 ± 9.50e-04	1.275e-02 ± 3.13e-03
		SplineFlow	4.187e-01 ± 5.87e-03	6.768e-01 ± 8.23e-03	1.423e-01 ± 1.72e-02	2.056e-02 ± 3.15e-03	1.514e-02 ± 5.15e-03
Damped Harmonic	0.25	SF2M	8.351e-01 ± 3.23e-02	9.505e-01 ± 2.01e-02	3.715e-01 ± 3.46e-02	3.297e-02 ± 7.30e-03	9.310e-02 ± 1.77e-02
		SplineFlow	7.987e-01 ± 1.57e-02	9.137e-01 ± 2.28e-02	3.646e-01 ± 2.11e-02	3.422e-02 ± 4.34e-03	9.169e-02 ± 1.07e-02
	0.5	SF2M	8.282e-01 ± 3.29e-02	9.727e-01 ± 2.54e-02	3.192e-01 ± 7.43e-03	2.205e-02 ± 2.68e-03	6.567e-02 ± 5.04e-03
		SplineFlow	8.050e-01 ± 8.73e-03	9.813e-01 ± 3.99e-02	3.210e-01 ± 2.84e-02	2.179e-02 ± 5.59e-03	6.875e-02 ± 1.21e-02
	0.75	SF2M	9.123e-01 ± 2.70e-02	1.156e+00 ± 3.93e-02	2.752e-01 ± 2.17e-02	1.096e-02 ± 2.14e-03	4.651e-02 ± 6.44e-03
		SplineFlow	9.378e-01 ± 2.89e-02	1.172e+00 ± 1.17e-02	2.857e-01 ± 1.10e-02	1.242e-02 ± 7.65e-04	5.279e-02 ± 4.89e-03
Lotka-Volterra	0.25	SF2M	4.072e-01 ± 6.92e-02	4.044e-01 ± 7.33e-02	4.002e-01 ± 2.56e-02	9.246e-02 ± 8.00e-03	3.457e-01 ± 3.23e-02
		SplineFlow	3.184e-01 ± 3.58e-02	3.211e-01 ± 3.21e-02	3.189e-01 ± 1.21e-02	4.448e-02 ± 5.03e-03	1.749e-01 ± 2.60e-02
	0.5	SF2M	3.500e-01 ± 2.88e-02	3.545e-01 ± 3.12e-02	3.745e-01 ± 3.69e-02	8.036e-02 ± 2.88e-02	2.931e-01 ± 9.23e-02
		SplineFlow	2.877e-01 ± 2.32e-02	2.851e-01 ± 2.54e-02	3.102e-01 ± 1.16e-02	4.419e-02 ± 3.80e-03	1.636e-01 ± 2.32e-02
	0.75	SF2M	5.241e-01 ± 1.24e-01	5.260e-01 ± 1.21e-01	4.463e-01 ± 9.53e-02	1.069e-01 ± 3.98e-02	4.158e-01 ± 1.58e-01
		SplineFlow	3.770e-01 ± 5.73e-02	3.785e-01 ± 5.48e-02	3.608e-01 ± 4.04e-02	5.570e-02 ± 9.43e-03	2.228e-01 ± 4.77e-02

Table 34. Performance of models on holdout interpolation and extrapolation setting for the brain regeneration Dataset.

Embedding	Task	Model	Wasserstein	MMD	Energy
PHATE	Interpolation	MOTFM	7.94e-1 ± 2.64e-2	5.03e-1 ± 1.60e-2	1.44e+0 ± 6.21e-2
		SF2M	7.53e-1 ± 2.58e-2	4.57e-1 ± 8.30e-3	1.31e+0 ± 3.55e-2
		SplineFlow	6.07e-1 ± 2.71e-2	2.85e-1 ± 6.60e-3	8.15e-1 ± 2.14e-2
	Extrapolation	MOTFM	1.57e+0 ± 4.50e-3	1.01e+0 ± 1.15e-2	3.89e+0 ± 5.07e-2
		SF2M	1.53e+0 ± 4.72e-2	9.72e-1 ± 9.20e-3	3.77e+0 ± 7.24e-2
		SplineFlow	1.59e+0 ± 1.92e-2	9.55e-1 ± 8.70e-3	3.74e+0 ± 4.24e-2
PCA	Interpolation	MOTFM	9.01e-1 ± 2.16e-2	7.12e-2 ± 4.40e-3	1.16e+0 ± 5.24e-2
		SF2M	8.88e-1 ± 7.40e-3	6.68e-2 ± 7.00e-4	1.14e+0 ± 1.24e-2
		SplineFlow	8.38e-1 ± 1.37e-2	5.82e-2 ± 2.50e-3	1.02e+0 ± 3.93e-2
	Extrapolation	MOTFM	7.99e-1 ± 3.10e-3	1.35e-1 ± 6.90e-3	1.65e+0 ± 4.28e-2
		SF2M	8.65e-1 ± 1.54e-2	1.77e-1 ± 2.50e-3	1.92e+0 ± 1.27e-2
		SplineFlow	8.04e-1 ± 3.72e-2	1.29e-1 ± 6.80e-3	1.65e+0 ± 5.66e-2

Table 35. Performance of models across holdout interpolation and extrapolation settings for the embryoid development dataset.

Embedding	Task	Model	Wasserstein	MMD	Energy
PHATE	Interpolation	MOTFM	3.78e-1 ± 1.11e-2	6.01e-2 ± 2.52e-3	1.75e-1 ± 4.98e-3
		SF2M	2.72e-1 ± 2.36e-2	2.46e-2 ± 4.03e-3	8.63e-2 ± 1.33e-2
		SplineFlow	2.07e-1 ± 1.69e-2	1.26e-2 ± 5.87e-4	3.96e-2 ± 1.40e-3
	Extrapolation	MOTFM	4.48e-1 ± 5.05e-2	8.25e-2 ± 9.05e-3	2.39e-1 ± 7.18e-3
		SF2M	4.39e-1 ± 4.40e-2	5.79e-2 ± 1.08e-2	1.94e-1 ± 1.57e-2
		SplineFlow	4.48e-1 ± 4.41e-2	6.90e-2 ± 1.70e-3	2.07e-1 ± 2.96e-2
PCA	Interpolation	MOTFM	2.86e-1 ± 1.37e-2	1.14e-2 ± 9.33e-4	1.65e-1 ± 1.23e-2
		SF2M	2.74e-1 ± 1.05e-2	9.12e-3 ± 8.42e-4	1.55e-1 ± 1.25e-2
		SplineFlow	2.96e-1 ± 1.46e-2	1.27e-2 ± 3.11e-4	1.99e-1 ± 9.34e-3
	Extrapolation	MOTFM	7.89e-1 ± 1.29e-1	3.75e-2 ± 2.11e-3	7.21e-1 ± 5.09e-2
		SF2M	5.92e-1 ± 2.02e-2	3.77e-2 ± 3.98e-4	7.47e-1 ± 1.18e-2
		SplineFlow	5.39e-1 ± 3.35e-2	3.58e-2 ± 4.42e-3	6.89e-1 ± 1.01e-1